

# Dual-radiotracer translational SPECT neuroimaging. Comparison of three methods for the simultaneous brain imaging of D<sub>2/3</sub> and 5-HT<sub>2A</sub> receptors

Stergios Tsartsalis<sup>a,b</sup>, Benjamin B. Tournier<sup>a</sup>, Selim Habiby<sup>a</sup>, Meriem Ben Hamadi<sup>a</sup>, Cristina Barca<sup>a</sup>, Nathalie Ginovart<sup>a,c</sup>, Philippe Millet<sup>a,c,\*</sup>

<sup>a</sup> Division of Adult Psychiatry, Department of Mental Health and Psychiatry, University Hospitals of Geneva, Switzerland

<sup>b</sup> Division of Addictology, Department of Mental Health and Psychiatry, University Hospitals of Geneva, Switzerland

<sup>c</sup> Department of Psychiatry, University of Geneva, Switzerland

## ARTICLE INFO

### Keywords:

IBZM  
SPECT  
D<sub>2/3</sub> receptor  
5-HT<sub>2A</sub> receptor  
Dual-radiotracer  
Simultaneous SPECT

## ABSTRACT

**Purpose:** SPECT imaging with two radiotracers at the same time is feasible if two different radioisotopes are employed, given their distinct energy emission spectra. In the case of <sup>123</sup>I and <sup>125</sup>I, dual SPECT imaging is not straightforward: <sup>123</sup>I emits photons at a principal energy emission spectrum of 143.1–179.9 keV. However, it also emits at a secondary energy spectrum (15–45 keV) that overlaps with the one of <sup>125</sup>I and the resulting cross-talk of emissions impedes the accurate quantification of <sup>125</sup>I. In this paper, we describe three different methods for the correction of this cross-talk and the simultaneous *in vivo* [<sup>123</sup>I]IBZM and [<sup>125</sup>I]R91150 imaging of D<sub>2/3</sub> and 5-HT<sub>2A</sub> receptors in the rat brain.

**Methods:** Three methods were evaluated for the correction of the effect of cross-talk in a series of simultaneous, [<sup>123</sup>I]IBZM and [<sup>125</sup>I]R91150 *in vivo* and phantom SPECT scans. Method 1 employs a dual-energy window (DEW) approach, in which the cross-talk on <sup>125</sup>I is considered a stable fraction of the energy emitted from <sup>123</sup>I at the principal emission spectrum. The coefficient describing the relationship between the emission of <sup>123</sup>I at the principal and the secondary spectrum was estimated from a series of single-radiotracer [<sup>123</sup>I]IBZM SPECT studies. In Method 2, spectral factor analysis (FA) is applied to separate the radioactivity from <sup>123</sup>I and <sup>125</sup>I on the basis of their distinct emission patterns across the energy spectrum. Method 3 uses a modified simplified reference tissue model (SRTM<sub>C</sub>) to describe the kinetics of [<sup>125</sup>I]R91150. It includes the coefficient describing the cross-talk on <sup>125</sup>I from <sup>123</sup>I in the model parameters. The results of the correction of cross-talk on [<sup>125</sup>I]R91150 binding potential (BP<sub>ND</sub>) with each of the three methods, using cerebellum as the reference region, were validated against the results of a series of single-radiotracer [<sup>123</sup>I]R91150 SPECT studies. In addition, the DEW approach (Method 1), considered to be the most straightforward to apply of the three, was further applied in a dual-radiotracer SPECT study of the relationship between D<sub>2/3</sub> and 5-HT<sub>2A</sub> receptor binding in the striatum, both at the voxel and at the regional level.

**Results:** Average regional BP<sub>ND</sub> values of [<sup>125</sup>I]R91150, estimated on the cross-talk corrected dual-radiotracer SPECT studies provided satisfactory correlations with the BP<sub>ND</sub> values for [<sup>123</sup>I]R91150 from single-radiotracer studies:  $r = 0.92$ ,  $p < 0.001$  for Method 1,  $r = 0.92$ ,  $p < 0.001$  for Method 2,  $r = 0.92$ ,  $p < 0.001$ , for Method 3. The coefficient describing the ratio of the <sup>123</sup>I-emitted radioactivity at the <sup>125</sup>I-emission spectrum to the radioactivity that it emits at its principal emission spectrum was 0.34 *in vivo*. Dual-radiotracer *in vivo* SPECT studies corrected with Method 1 demonstrated a positive correlation between D<sub>2/3</sub> and 5-HT<sub>2A</sub> receptor binding in the rat nucleus accumbens at the voxel level. At the VOI-level, a positive correlation was confirmed in the same region ( $r = 0.78$ ,  $p < 0.01$ ).

**Conclusion:** Dual-radiotracer SPECT imaging using <sup>123</sup>I and <sup>125</sup>I-labeled radiotracers is feasible if the cross-talk of <sup>123</sup>I on the <sup>125</sup>I emission spectrum is properly corrected. The most straightforward approach is Method 1, in which a fraction (34%) of the radioactivity emitted from <sup>123</sup>I at its principal energy spectrum is subtracted from the measured radioactivity at the spectrum of <sup>125</sup>I. With this method, a positive correlation between the binding of [<sup>123</sup>I]IBZM and [<sup>125</sup>I]R91150 was demonstrated in the rat nucleus accumbens. This result highlights the interest

\* Corresponding author. Division of Adult Psychiatry, Department of Psychiatry, University Hospitals of Geneva Switzerland, Chemin du Petit-Bel-Air 2, CH1225, Chêne-Bourg, Switzerland.

E-mail address: [Philippe.Millet@hcuge.ch](mailto:Philippe.Millet@hcuge.ch) (P. Millet).

<https://doi.org/10.1016/j.neuroimage.2018.04.063>

Received 30 October 2017; Received in revised form 11 March 2018; Accepted 27 April 2018

Available online 30 April 2018

1053-8119/© 2018 Elsevier Inc. All rights reserved.

of dual-radiotracer SPECT imaging to study multiple neurotransmitter systems at the same time and under the same biological conditions.

## Introduction

Molecular neuroimaging permits the study of brain function in health and disease. Radiotracers targeting a wide panel of neurobiological processes have been developed: regarding the neurotransmitter systems, single-photon emission computed tomography (SPECT) and positron emission tomography (PET) studies provide knowledge on neuroreceptor levels, receptor-neurotransmitter-interactions, endogenous neurotransmitter levels etc. (Frankle et al., 2005; Laruelle, 2000). With the advent of modern small-animal scanners, molecular imaging is now employed in the study of animal models of neuropsychiatric diseases. The advantage of using the same techniques in fundamental as in clinical research lies on the fact that animal models may provide insight into mechanistic aspects of human disease while the knowledge obtained from small-animal imaging may be more directly implemented in human research (Cunha et al., 2014; Frankle and Laruelle, 2002; Meikle et al., 2005; Nestler and Hyman, 2010; Xi et al., 2011).

Given the arsenal of radiotracers available in molecular neuroimaging, multiple biological targets may be studied on the same subject and permit a more thorough evaluation of brain physiology and pathology (Cselenyi et al., 2004; Fakhri, 2012). For example, a joint evaluation of D<sub>2/3</sub> and 5-HT<sub>2A</sub> receptors would be of interest for the study of schizophrenia as both receptors are implicated in the pathophysiology of the disease and a target for multiple antipsychotic agents (Ginovart and Kapur, 2012; Howes et al., 2012; Selvaraj et al., 2014). Another highly interesting example of joint exploration of multiple biomarkers would be in dementia imaging (Jack et al., 2013). However, studying multiple targets on the same animal is technically difficult. Multiple scan sessions are time-consuming as they may need to be separated by various amounts of time for the radioisotope of the first scan to decay before the second scan and thus prevent bias in the radioactivity measurements. However, studying two or more biological phenomena using scan sessions that are separated by hours or even days may induce variability and bias due to the dynamic nature of most of biological phenomena that may rapidly evolve or even depend on each other (Fakhri, 2012). For instance, results from neuroreceptor studies may be subject to the effect of endogenous ligand binding to the receptors (Laruelle, 2000), which is a dynamic phenomenon, subject to physiological variations. Other parameters, such as the effect of anesthetic agents may alter the radiotracers' binding (McCormick et al., 2011) and thus hamper the joint interpretation of two phenomena under study unless they are studied at the exact same time, thus under the exact same conditions. Furthermore, multiple scan sessions may reduce the throughput of small animal imaging studies. Given the limitations described above, the development of simultaneous, dual-radiotracer molecular imaging could optimize biological studies both in terms of technical feasibility and of biological understanding of brain function (Fakhri, 2012).

Simultaneous, dual-radiotracer molecular imaging is theoretically feasible in SPECT. Each radioisotope used in SPECT emits photons in a particular energy spectrum. Two (or more) radioisotopes may thus be simultaneously employed in a single scan session and their respective radioactive signals be distinguished based on their emission spectra (Akutsu et al., 2009; Antunes et al., 1992; Bruce et al., 2000; Ichihara et al., 1993). This is the case for two iodine isotopes used in SPECT. <sup>123</sup>I has a principal energy emission spectrum of 143.1–179.9 keV and <sup>125</sup>I an energy spectrum of 15–45 keV. The majority of radiotracers used in SPECT studies of the central nervous system (CNS) is radioiodinated (Baeken et al., 1998; De Bruyne et al., 2010; Dumas et al., 2014, 2015; Ji et al., 2015; Kessler et al., 1991; Kung et al., 1989; Mattner et al., 2008, 2011; Ordonez et al., 2015; Pimlott and Ebmeier, 2007; Sehlin et al., 2016; Tsartsalis et al., 2014a, 2015) and the possibility to perform

dual-radiotracer SPECT using <sup>123</sup>I and <sup>125</sup>I would thus be of interest for a wide spectrum of *in vivo* studies in animal models of neuropsychiatric conditions. Nevertheless, distinction of <sup>123</sup>I- and <sup>125</sup>I-emitted photons is not straightforward: <sup>123</sup>I emits at a secondary energy spectrum that overlaps with the one of <sup>125</sup>I and the resulting cross-talk of emissions impedes the accurate quantification of <sup>125</sup>I.

In this paper, we compare three different methods for the correction of cross-talk between <sup>123</sup>I and <sup>125</sup>I and apply them to the simultaneous quantification of D<sub>2/3</sub> and 5-HT<sub>2A</sub> receptors, using the [<sup>123</sup>I]IBZM and [<sup>125</sup>I]R91150, respectively. Furthermore, we apply this methodology to study the relationship between the [<sup>123</sup>I]IBZM and [<sup>125</sup>I]R91150 binding in the rat striatum and thus illustrate the potential of dual-radiotracer imaging for *in vivo* biological studies of brain function and pathology.

## Materials and methods

### <sup>123</sup>I and <sup>125</sup>I phantom SPECT studies

Eighteen groups of three cylindrical phantoms each (2 ml Eppendorf® tubes) were prepared. In each group, one tube was filled with a solution containing <sup>123</sup>I (GE Healthcare, Eindhoven, Netherlands), one with the same radioactive concentration of <sup>125</sup>I (Perkinelmer, Schwerzenbach, Suisse) and a third tube with a mixture of equal concentrations of both radioisotopes (each radioisotope at half the quantity of radioactivity in the adjacent single radioisotope-containing tube). Attention was paid for the tubes to be filled with the exact same radioactive concentration so that the measurement in the single-radioisotope containing tubes to be exactly twice the radioactivity of the same radioisotope in the tubes containing both. In this way, the measurements in the single radioisotope-containing tubes could serve as controls for the measurement in the dual-radioisotope containing tubes after correction for cross-talk. Radioactive concentrations varied from 0.9 to 3.5 MBq/ml. The tubes of each group were positioned along the longitudinal axis of the U-SCAN-II SPECT camera (MiLabs, Utrecht, Netherlands) on a rectangular polystyrene scaffold. A 10-min static SPECT acquisition was performed.

### Radiotracer preparation

All chemicals were purchased from Sigma-Aldrich (Buchs, Switzerland) with the highest purity available, unless otherwise specified. [<sup>123</sup>I]IBZM was obtained by incubation, for 15 min at 68 °C, of a mixture containing 5 µL of BZM precursor (ABX, Germany, 24 nmol/µl in ethanol), 2 µL of glacial acetic acid, 1 µL of 30% H<sub>2</sub>O<sub>2</sub> and 10 mCi of carrier-free <sup>123</sup>I sodium iodide in 0.05 M NaOH (GE Healthcare, Eindhoven, Netherlands). The radiotracer was isolated by a linear gradient HPLC run (from 5% acetonitrile, ACN, to 95% ACN, 10 mM H<sub>3</sub>PO<sub>4</sub>, in 10 min).

For R91150 radiolabeling, 300 µg of R91150 precursor in 3 µL ethanol was mixed with 3 µL of glacial acetic acid, 15 µL of carrier-free <sup>123</sup>I or <sup>125</sup>I (Perkin Elmer) sodium iodide (10 mCi) in 0.05 M NaOH, and 3 µL of 30% H<sub>2</sub>O<sub>2</sub>. [<sup>123</sup>I]R91150/[<sup>125</sup>I]R91150 was isolated by an isocratic HPLC run (ACN/water 50/50, 10 mM acetic acid buffer) with a reversed-phase column (Bondclone C18 10 µm 300 × 7.8 mm, Phenomenex, Schlieren, Switzerland) at a flow rate of 3 ml/min. Radiochemical purity, assessed by HPLC, was above 98% (Dumas et al., 2014).

### *In vivo* SPECT studies and scan procedures

Thirty-two male *Mdr1a* KO rats (SD-Abcbl1tm1sage, Sigma Advance Genetic Engineering Labs, USA), weighing 370–573 g were used. Their repartition was as follows: 1) Three rats were used in a single-radiotracer

[<sup>123</sup>I]IBZM SPECT study. This study allowed the estimation of the  $\alpha$  coefficient describing the relationship between the emission of [<sup>123</sup>I]IBZM at the 15–45 keV spectrum and the emission of the same radiotracer at the 143,1–179,9 keV spectrum (see section 2.5.1 for more detail). 2) Four rats were used in a single-radiotracer [<sup>123</sup>I]R91150 study and the results of the quantification were used as “ground truth” for the validation of the results of cross-talk correction in dual-radiotracer SPECT studies. 3) Three rats were employed in a simultaneous, dual-radiotracer SPECT study to validate the three different methods of correction of the cross-talk between [<sup>123</sup>I]IBZM and [<sup>125</sup>I]R91150 by comparing the results of quantification with the results of study 2. 4) Ten rats were used in a dual-radiotracer [<sup>123</sup>I]IBZM and [<sup>125</sup>I]R91150 study to evaluate the test-retest reliability of the quantification of D<sub>2/3</sub> and 5-HT<sub>2A</sub> receptors with this protocol. In addition, with these ten rats, the correlation between these two receptors in the nucleus accumbens (NAcc) was studied. 5) In a supplemental study, one rat was employed in a dual-radiotracer study in which [<sup>123</sup>I]R91150 was labeled with <sup>123</sup>I and [<sup>125</sup>I]IBZM with <sup>125</sup>I. 6) Finally, eight rats were used in a supplemental *in vitro* study of D<sub>2/3</sub> and 5-HT<sub>2A</sub> quantification in the NAcc to validate the results of the *in vivo* study. Table 1 summarizes the above description. All experimental procedures were performed in accordance with the Swiss Federal Law on animal care under a protocol approved by the Ethical Committee on Animal Experimentation of the Canton of Geneva, Switzerland.

SPECT scans were performed under isoflurane anesthesia (4% for induction, 2.5% for maintenance). Body temperature was maintained at 37 ± 1 °C by means of a thermostatically controlled heating blanket. A polyethylene catheter (22G) was inserted in the tail vein for radiotracer injection, at a volume of 0.6 ml over a 1-min period using an infusion pump. The scan protocol, regarding the number of image-frames is presented for each study in Table 1.

**Table 1**  
Repartition of rats into experimental groups.

Experiment	n	SPECT protocol	Objective/Outcome measures
1. Single-radiotracer [ <sup>123</sup> I]IBZM study	3	120 x 1-min frames	Estimation of $\alpha$ coefficient Estimation of BP <sub>ND</sub> (SUR)
2. Single-radiotracer [ <sup>123</sup> I]R91150 study	4	120 x 1-min frames	Estimation of BP <sub>ND</sub> (SUR)
3. Dual-radiotracer [ <sup>123</sup> I]IBZM/[ <sup>125</sup> I]R91150 validation study	3	240 x 1-min frames, ( <sup>125</sup> I]R91150 injected at t = 0 and [ <sup>123</sup> I]IBZM injected at t = 20 min)	Validation of BP <sub>ND</sub> estimation with SUR after cross-talk correction with DEW/Spectral FA/SRTM <sub>C</sub>
4. Study of the D <sub>2/3</sub> -5-HT <sub>2A</sub> binding in striatum and test-retest variability assessment	10	4 × 10-min frames scan, initiated at t = 80 min after the simultaneous injection of [ <sup>123</sup> I]IBZM/[ <sup>125</sup> I]R91150	Estimation of BP <sub>ND</sub> (SUR) after DEW-correction for cross-talk/Test-retest variability/correlation between D <sub>2/3</sub> -5-HT <sub>2A</sub>
5. Supplemental experiment Dual-radiotracer [ <sup>123</sup> I]R91150/[ <sup>125</sup> I]IBZM validation study	1	240 x 1-min frames, ( <sup>125</sup> I]IBZM injected at t = 0 and [ <sup>123</sup> I]R91150 injected at t = 20 min)	Evaluation of a possible bias of [ <sup>123</sup> I]R91150 on [ <sup>125</sup> I]IBZM
6. Supplemental experiment Single-radiotracer [ <sup>125</sup> I]R91150 study	3	1 × 20-min frame, (initiated at t = 100 min after [ <sup>125</sup> I]R91150 injection)	Evaluation of a possible bias in BP <sub>ND</sub> due to the use of <sup>125</sup> I
7. Supplemental experiment <i>In vitro</i> autoradiography study of D <sub>2/3</sub> and 5-HT <sub>2A</sub> binding	8	–	Estimation of 1) D <sub>2/3</sub> binding in brain slices from frontal cortical and striatal regions and 2) 5-HT <sub>2A</sub> binding onto immediately adjacent slices

SPECT image reconstruction, co-registration and regional radioactivity measurement extraction

SPECT image reconstruction from phantom and *in vivo* rat studies (single- and dual-radiotracer) was performed using a pixel ordered subsets expectation maximization (P-OSEM, 0.4 mm voxels, 4 iterations, 6 subsets) algorithm using MiLabs image reconstruction software. Reconstruction of dynamic SPECT images was performed using the radioactivity measured at each radioisotope's principal energy spectrum, that is at 143,1–179,9 keV for <sup>123</sup>I and at 15–45 keV for <sup>125</sup>I. Reconstruction of static SPECT images was performed at the aforementioned energy spectra but also over the whole energy spectrum from 0 to 200 keV, with 5 keV-wide windows (in this case, image-volumes containing the reconstructions of a static SPECT image over the whole spectrum are termed “spectral images”). In this way, the pattern of emission of each radioisotope over the whole energy spectrum is studied. Radioactive decay correction was performed while correction for attenuation or scatter was not.

SPECT images were processed using PMOD software (version 3.8, 2014, PMOD Technologies Ltd, Zurich, Switzerland). Radioactivity from the phantom study (section 2.1) was extracted from the SPECT image by means of an ellipsoid volume-of-interest (VOI) manually placed at the center of the tube (2 cm<sup>3</sup>). *In vivo* SPECT scans were manually co-registered to a rat MRI and a VOI template (including 57 VOIs), incorporated in PMOD (Schiffer et al., 2006). In the case of dynamic SPECT images, manual co-registration was performed on images of average radioactivity over many frames of acquisition, to enhance the visualization of the brain. Co-registration parameters of these averaged images were then applied to individual frames of the dynamic images and time-activity-curves (TACs) were generated.

Simultaneous dual-radiotracer SPECT signal separation

For the dual-radiotracer study, a 240 x 1-min frame SPECT acquisition started immediately after a [<sup>125</sup>I]R91150 injection at t = 0 (62.88 ± 19.14 MBq), while [<sup>123</sup>I]IBZM was injected at t = 20 min (66.33 ± 26.02 MBq). The protocol for the dual-radiotracer studies is presented in Fig. 1. For the single radiotracer studies, a 120 x 1-min frame SPECT acquisition was initiated upon radiotracer injection. Radioactive concentration at the time of injection was 100.45 ± 34.15 MBq for the single-radiotracer [<sup>123</sup>I]R91150 study and 90.45 ± 3.27 MBq for the single-radiotracer [<sup>123</sup>I]IBZM study. Three different methods of signal separation in dual-radiotracer SPECT were employed in this paper:

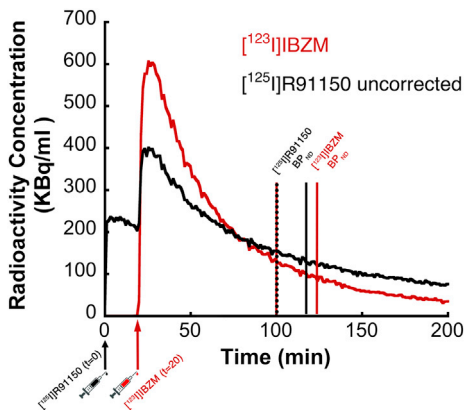


**Fig. 1.** The protocol employed in the dual-radiotracer experiments (as described in section 2.3). The SPECT scan starts with an injection of [<sup>125</sup>I]R91150, followed by the injection of [<sup>123</sup>I]IBZM, 20 min later. The [<sup>125</sup>I]R91150 TAC is unbiased until the moment of [<sup>123</sup>I]IBZM injection. The time-windows on which the BP<sub>ND</sub> values for the two radiotracers is estimated, are indicated with the vertical lines.

**Method 1: correction of the cross-talk between  $^{123}\text{I}$  and  $^{125}\text{I}$  by subtracting the  $^{123}\text{I}$ -derived contamination from the  $^{125}\text{I}$  radioactive signal (hereon, dual energy window method)**

Lee and colleagues (Lee et al., 2013, 2015) proposed a dual energy window (DEW) method, exploiting the fact that the emission of  $^{123}\text{I}$  at the principal (high) energy spectrum at 143.1–179.9 keV and the emission at the secondary (low) energy spectrum at 15–45 keV (this one producing the cross-talk with  $^{125}\text{I}$ ) have a linear relationship, described by the following equation:

$$^{123}\text{I}_{\text{low}} = \alpha * ^{123}\text{I}_{\text{high}} \quad (1)$$

where  $^{123}\text{I}_{\text{low}}$  and  $^{123}\text{I}_{\text{high}}$  denote the radioactivity of the low and high-energy emission spectra, respectively and  $\alpha$  is an unknown coefficient. The  $\alpha$  coefficient was estimated from the  $^{123}\text{I}$  phantom study (section 2.1) and the *in vivo* single-radiotracer [ $^{123}\text{I}$ ]IBZM SPECT study (section 2.5). It was given by fitting equation (1) to the scatter plot of the radioactivity measured at the high-energy spectrum and the corresponding measurement at the low-energy spectrum, across  $^{123}\text{I}$  phantoms. For the *in vivo* imaging study, the  $\alpha$  coefficient was estimated by fitting equation (1) to the radioactivity measured at the high-energy spectrum and the corresponding measurement at the low-energy spectrum, in each of the 57 VOIs over the three rats of the single-radiotracer [ $^{123}\text{I}$ ]IBZM study (section 2.3).

Knowing the  $\alpha$  coefficient permits to correct the total radioactivity measured at the low-energy window ( $^{125/123}\text{I}$ ), where the cross-talk between  $^{123}\text{I}$  and  $^{125}\text{I}$  is observed. Indeed, in this case, the radioactivity emitted by  $^{125}\text{I}$  only ( $^{125}\text{I}$ ) will be given by the following equation:

$$^{125}\text{I} = ^{125/123}\text{I} - \alpha * ^{123}\text{I}_{\text{high}} \quad (2)$$

all other parameters are known, including the radioactivity measured at the high-energy spectrum ( $^{123}\text{I}_{\text{high}}$ ), which is not influenced by cross-talk and directly quantified. After application of the DEW method, the non-displaceable binding potential ( $\text{BP}_{\text{ND}}$ ) (Innis et al., 2007) was estimated on static images corresponding to acquisitions between the 80th and the 110th min after injection for the [ $^{123}\text{I}$ ]IBZM studies and between the 100th and the 120th min after injection for [ $^{125}\text{I}$ ]R91150. These time-windows correspond to pseudo-equilibrium conditions and permit a simple specific uptake ratio method (SUR) to be used for  $\text{BP}_{\text{ND}}$  estimation, as previously demonstrated ( $\text{BP}_{\text{ND}} = \text{Radioactivity in target region} / \text{Radioactivity in reference region} - 1$ ) (Dumas et al., 2015; Tsartsalis et al., 2017). These time-windows were employed whenever the estimation of  $\text{BP}_{\text{ND}}$  was performed over static SPECT images with the SUR method in this paper.

#### Method 2: spectral factor analysis (FA)

As described in section 2.4, static images from phantom and *in vivo* experiments were reconstructed across the energy spectrum in 5 keV-wide energy windows and all these reconstructed images were combined in a single volume, termed a spectral image, one for each phantom or rat. Spectral images were processed in the Pixies software (Apteryx, Issy-les-Moulineaux, France) as previously described (Di Paola et al., 1982; Millet et al., 2012; Tsartsalis et al., 2014a). In this paper, FA is used for the decomposition of spectral images into a few elementary component-images, each one of them representing the emission pattern of one radioisotope over the emission spectrum. The decomposition is based on the distinct spectral pattern of each component-image and is performed at the voxel level. The objective is to distinguish the radioactive signal with respect to the radioisotope ( $^{123}\text{I}$  or  $^{125}\text{I}$ ) that emitted it. Thus, the emission pattern of radioactivity in each voxel ( $i$ ) of an original (raw) spectral image,  $V_i^{\text{raw}}(r)$  (where  $r$  is the energy window at which reconstruction was performed), is expressed as a function of a finite number ( $k$ ) of curves called factors  $f_k$ , each one corresponding to a distinct radioactivity emission pattern across the energy spectrum and a set of factor-images  $M_k$  that represent the spatial distribution of the

factors. Overall, the decomposition of the radioactive signal may be expressed using the following equation:

$$V_i^{\text{raw}}(r) = \sum_{k=1}^K M_k(i)f_k(r) + e_i(r) \quad (3)$$

where  $e_i(r)$  represents the error term for each voxel ( $i$ ) at energy ( $r$ ) including both noise and modeling errors. In the present study,  $K = 3$ , given that we know *a priori* that the whole radioactive signal is emitted by two radioisotopes and the third factor corresponds to the data that is not attributed to either  $^{123}\text{I}$ - or  $^{125}\text{I}$ -emitted signal. In addition, the distinct pattern of emission from each radiotracer over the energy spectrum is known from the reconstruction of the single-radiotracer images (section 2.1) that contained only one of the radioisotopes at a time. This *a priori* known pattern of emission was employed as a constraint of similitude in FA, i.e. obliging the software to extract factors similar to the known patterns of emission of  $^{123}\text{I}$  and  $^{125}\text{I}$ . For a more detailed description of FA and the application of a constraint of similitude, please see (Millet et al., 2012). After FA, the images corresponding to the factor representing  $^{125}\text{I}$  and more precisely its emission spectrum at 15–45 keV were extracted and considered cross-talk-corrected.  $\text{BP}_{\text{ND}}$  was estimated over [ $^{123}\text{I}$ ]IBZM and [ $^{125}\text{I}$ ]R91150 SPECT images with the SUR method.

#### Method 3: inclusion of the effect of cross-talk in the compartmental analysis

Correction of the effect of cross-talk was also performed by including it in the equation of the simplified reference-tissue model (SRTM) (Lammertsma and Hume, 1996; Wu and Carson, 2002), as previously described (Carson et al., 2003; Tsartsalis et al., 2014b). The SRTM equation is the following:

$$C_{\text{VOI}}(t) = R_1 C_{\text{REF}}(t) + (k_2 - R_1 k_2 / (1 + \text{BP}_{\text{ND}})) C_{\text{REF}}(t) \otimes e^{-k_2 / (1 + \text{BP}_{\text{ND}}) t} \quad (4)$$

where  $C_{\text{VOI}}(t)$  and  $C_{\text{REF}}(t)$  are the TACs in the VOI and the reference region, respectively,  $R_1$  is the relative delivery of the radiotracer in the VOI with respect to the reference region ( $K_1/K_1'$ ),  $k_2$  are tissue efflux constants in the VOI.

In the present study, the radioactive signal measured at 15–45 keV corresponds to [ $^{125}\text{I}$ ]R91150 and a part of the [ $^{123}\text{I}$ ]IBZM signal as a result of cross-talk. Taken equation (2) into account, at any time point

$$C_{\text{VOI}}^{125}(t) = C_{\text{VOI}}^{\text{total}}(t) - \alpha C_{\text{VOI}}^{123}(t) \quad (5)$$

and

$$C_{\text{REF}}^{125}(t) = C_{\text{REF}}^{\text{total}}(t) - \alpha' C_{\text{REF}}^{123}(t) \quad (6)$$

where  $C_{\text{VOI}}^{125}(t)$  and  $C_{\text{REF}}^{125}(t)$  are the true TACs corresponding to [ $^{125}\text{I}$ ]R91150 in the VOI and reference region,  $C_{\text{VOI}}^{\text{total}}(t)$  and  $C_{\text{REF}}^{\text{total}}(t)$  correspond to the measured TAC, that includes the cross-talk from [ $^{123}\text{I}$ ]IBZM,  $C_{\text{VOI}}^{123}(t)$  and  $C_{\text{REF}}^{123}(t)$  are measured radioactivities at the  $^{123}\text{I}$  principal emission spectrum in the VOI and reference region, respectively. The  $\alpha$  parameter, corresponding to the VOIs, is fitted. On the other hand, considering the reference region ( $\alpha'$ ) it is fixed with the value estimated as described in section 2.5.1.

Combining equations (4)–(6) gives the operational equation of the “corrected” SRTM or  $\text{SRTM}_{\text{C}}$ :

$$C_{\text{VOI}}^{\text{total}}(t) = R_1 (C_{\text{REF}}^{\text{total}}(t) - \alpha' C_{\text{REF}}^{123}(t)) + (k_2 - R_1 k_2 / (1 + \text{BP}_{\text{ND}})) (C_{\text{REF}}^{\text{total}}(t) - \alpha' C_{\text{REF}}^{123}(t)) \otimes e^{-\frac{k_2}{(1 + \text{BP}_{\text{ND}})} t} + \alpha C_{\text{VOI}}^{123}(t) \quad (7)$$

that was implemented in PMOD software, as previously described (Tsartsalis et al., 2014b). Thus, the number of parameters to fit with  $\text{SRTM}_{\text{C}}$  is one more than in the SRTM, which is the  $\alpha$  coefficient for every VOI (given that for the reference region it is fixed (Tsartsalis et al., 2014b)).

## Statistical analysis

In phantom experiments, radioactivity measurements from cross-talk corrected images of phantoms that contained both radioisotopes were compared to measurements from the respective adjacent phantoms containing a single radioisotope. In rat experiments, regional BP<sub>ND</sub> values resulting from the quantification of cross-talk-corrected dual-radiotracer images, were compared with corresponding values from single-radiotracer images of *in vivo* experiments. Comparisons in both cases were performed by means of linear regression analysis and paired-sampled *t*-test. Statistical significance was set to  $p < 0.05$ .

## Evaluation of the relationship between striatal D<sub>2/3</sub> and 5-HT<sub>2A</sub>-receptor binding at the voxel and VOI level

The relationship between D<sub>2/3</sub> and 5-HT<sub>2A</sub> binding in the striatum has been evaluated in an independent group of ten Mdr1a KO rats, weighing 370–520 g. SPECT scans and image reconstruction were performed as described in sections 2.3 and 2.4, respectively, with the difference that a shorter scanning protocol was employed: a scan composed of four, 10 min-long frames was initiated at  $t = 80$  after a concurrent injection of  $30.42 \pm 8.92$  MBq of [<sup>123</sup>I]IBZM and  $24.6 \pm 5.63$  MBq of [<sup>125</sup>I]R91150. In this experiment, no time interval was left between the injections of the two radiotracers, contrary to the dual-radiotracer studies described in section 2.3. In that case, the interval served in the dynamic SPECT protocol and the SRTM<sub>C</sub> method, to demonstrate the effect of cross-talk on the radiotracer's kinetics. Dual-radiotracer imaging was performed using the DEW method (Method 1 in section 2.5.1) and BP<sub>ND</sub> was estimated as in section 2.5.1 with the SUR over frames corresponding to 80–110 min post radiotracer injection for [<sup>123</sup>I]IBZM and 100–120 min for [<sup>125</sup>I]R91150. A test-retest analysis of BP<sub>ND</sub> estimations using this approach is described in the supplemental material. To perform voxel-wise linear regression analysis between D<sub>2/3</sub> and 5-HT<sub>2A</sub> receptor binding across the group of six rats, static SPECT images corresponding to 80–110 min post radiotracer injection for [<sup>123</sup>I]IBZM and 100–120 min for [<sup>125</sup>I]R91150 were spatially normalized as follows: at first, a [<sup>125</sup>I]R91150 template-image was created with the Small Animal Molecular Imaging Toolbox (Vallez Garcia et al., 2015) (SAMIT, Groningen, Netherlands) using the static [<sup>125</sup>I]R91150 SPECT scans mentioned above, in Matlab (R2016,

Mathworks Inc, USA). Then, spatial normalization of the [<sup>125</sup>I]R91150 SPECT images of each rat was performed in PMOD, which implements methods according to SPM5 software (Wellcome Trust Center for Neuroimaging, UCL, London, UK). The resulting transformation matrix was applied to the corresponding [<sup>123</sup>I]IBZM images. Then, voxel-wise regression analysis of [<sup>123</sup>I]IBZM and [<sup>125</sup>I]R91150 binding was performed in Matlab (estimated using the SUR) and images of the Pearson's *r* coefficient and associated *p*-values were produced. Linear regression analysis was also performed at the VOI level (in the NAcc and the caudate/putamen nucleus, CPU, bilaterally) on these same parametric images of BP<sub>ND</sub>. An experimental and simulation study to validate that the observed correlation between D<sub>2/3</sub> and 5-HT<sub>2A</sub> binding is not due to any residual cross-talk activity from [<sup>123</sup>I]IBZM on [<sup>125</sup>I]R91150 images is described in the supplemental material.

## Results

In Fig. 1, the protocol used in the dual-radiotracer experiments (see section 2.3) is presented. The [<sup>125</sup>I]R91150 TAC is unbiased until the 20th min, when [<sup>123</sup>I]IBZM is injected. From this moment on, the [<sup>125</sup>I]R91150 TAC is considerably biased for the whole duration of the experiment. The effect of cross-talk on the radioactivity measurements at the low-energy spectrum is also presented in Fig. 2. Indeed, in Fig. 2A, the SPECT image of the three phantoms was reconstructed at the low-energy window, in which both <sup>123</sup>I and <sup>125</sup>I are visualized. The emission from the <sup>123</sup>I-containing phantom shows that <sup>123</sup>I emits a considerable radioactive signal at this energy spectrum thus producing the cross-talk phenomenon with the <sup>125</sup>I-derived radioactivity.

## Correction of the cross-talk between <sup>123</sup>I and <sup>125</sup>I with the DEW method

Fig. 3A depicts the radioactivity measured in a <sup>123</sup>I-phantom SPECT experiment across the energy spectrum. The radioactive counts measured from the <sup>123</sup>I phantoms at the high- (<sup>123</sup>I<sub>high</sub>) and the low-energy spectra (<sup>123</sup>I<sub>low</sub>) highly correlated with each other (Fig. 3B,  $r = 0.99$ ,  $p < 0.001$ ). The  $\alpha$  coefficient was found to be 0.58 in the phantom experiments. Fig. 3C depicts an image of three of the dual-radiotracer phantoms reconstructed at the low-energy spectrum before the correction for cross talk. In Fig. 3D, the images have been reconstructed at the high-energy

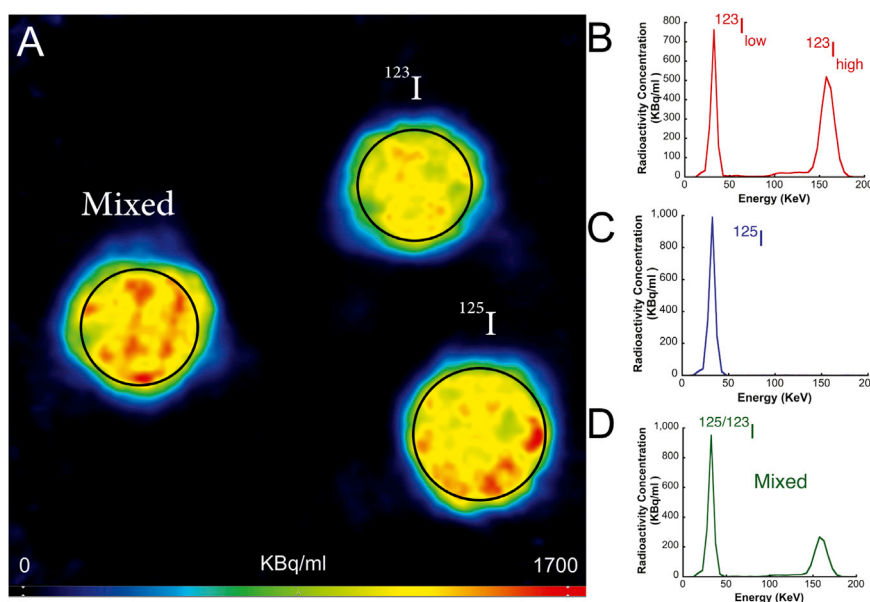


**Fig. 2.** (A) A static SPECT image from three phantoms filled with <sup>123</sup>I, <sup>125</sup>I and both (“Mixed”) radioisotopes, reconstructed at the low energy spectrum. The respective radioactive emissions across the energy spectrum are shown in (B–D). The double emission of <sup>123</sup>I, at the high and low spectra, the latter one overlaps with the <sup>125</sup>I spectrum and is at the origin of the cross-talk.

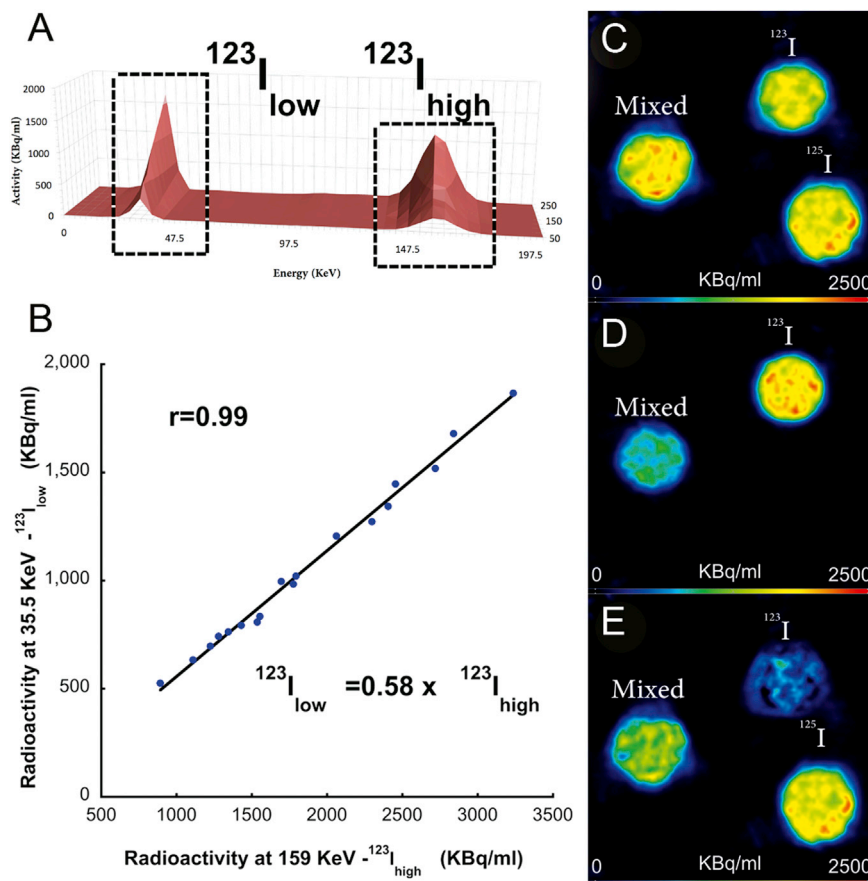


**Fig. 3.** (A) The radioactivity emission of  $^{123}\text{I}$ , across the energy spectrum. The radioactivity measured at the high ( $^{123}\text{I}_{\text{high}}$ ) and the low energy spectrum ( $^{123}\text{I}_{\text{low}}$ ) is noted on the plot. (B) linear regression between  $^{123}\text{I}_{\text{high}}$  and  $^{123}\text{I}_{\text{low}}$  for all the phantoms and estimation of the  $\alpha$  coefficient from the slope of the regression line (0.58). (C) An image of three phantoms reconstructed at the low energy window. (D) the same image reconstructed at the high energy window. (E) the same image reconstructed at the low energy window, corrected for cross-talk with the DEW method.

window, clearly demonstrating the disappearance of the  $^{125}\text{I}$ -containing phantom and the diminution in the activity in the mixed-radioactivity tube that contains both radioisotopes. In Fig. 3E, the image has been corrected for cross-talk with the DEW method. This led to an almost-disappearance of the  $^{123}\text{I}$ -containing phantom and a similar decrease in the radioactivity measured in the phantom containing both radioisotopes.

Fig. 4 A presents the corrected  $^{125}\text{I}$ R91150 image from an *in vivo* dual-radiotracer experiment. The images acquired correspond to the window between the 100th and the 120th minute post-injection. The predominance of binding in frontal cortical areas with respect to subcortical structures is observed, along with a fronto-caudal gradient in binding, a pattern typical of 5-HT<sub>2A</sub> distribution (Tsartsalis et al., 2016a). In Fig. 4B, the good correlation between the radioactive counts emitted

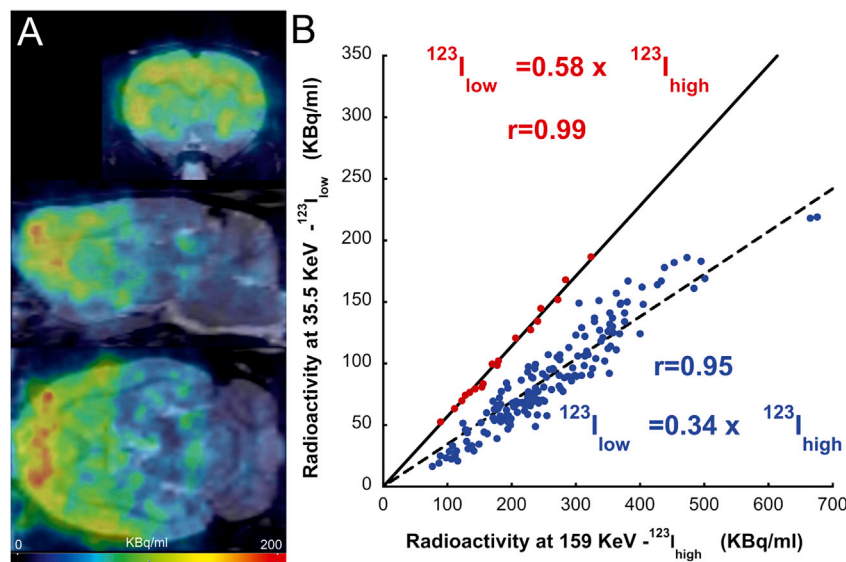


**Fig. 4.** (A) Coronal, sagittal and axial planes of a DEW-corrected *in vivo*  $^{125}\text{I}$ R91150 SPECT image. (B) The correlation between the radioactivity emitted from  $^{123}\text{I}$  IBZM at the high and the low energy spectra is plotted in blue dots. Each one of them corresponds to the measurements in one of the 57 brain VOIs in three rats *in vivo*. The correlation between the high and low energy emission of  $^{123}\text{I}$  as measured in phantom experiments (shown in Fig. 3B) is also shown in red dots.

by [ $^{123}\text{I}$ ]IBZM *in vivo* at the high- and the low-energy spectrum across the brain VOIs is presented ( $r = 0.95$ ,  $p < 0.001$ ). The same correlation from the phantom experiments is included for comparison. The  $\alpha$  coefficient was  $0.34 \pm 0.057$  *in vivo* for all VOI and across the three rats. The variability of the  $\alpha$  coefficient values was mainly due to some low-binding VOI. On the contrary, high binding VOI, striatal VOI and the CER, had less variable  $\alpha$  coefficient values ( $0.33 \pm 0.04$  in the motor cortex, MC,  $0.36 \pm 0.04$  in the medial prefrontal cortex, MPFC,  $0.30 \pm 0.02$  in the orbitofrontal cortex, OFC,  $0.35 \pm 0.04$  in the somatosensory cortex, SSC,  $0.31 \pm 0.04$  in the cingulate cortex, CC,  $0.35 \pm 0.03$  in the NAcc,  $0.33 \pm 0.02$  in the Caudate/Putamen, CPU and  $0.34 \pm 0.03$  in the CER).

#### Correction of the cross-talk between $^{123}\text{I}$ and $^{125}\text{I}$ using spectral FA

Fig. 5 shows the result of the application of spectral FA to correct for the effect of cross-talk on  $^{125}\text{I}$  signal in a phantom dual-radiotracer experiment. The factor-images corresponding to the  $^{123}\text{I}$ - and  $^{125}\text{I}$ -emitted radioactive signal and the third factor (Fig. 5A, C and 5E, respectively) are presented along with their respective factor-curves (Fig. 5B, D and 5F). In Fig. 5A, in which the  $^{123}\text{I}$ -emitted signal is retained, the  $^{125}\text{I}$ -containing phantom virtually disappears and the opposite is observed in Fig. 5C, where  $^{125}\text{I}$ -emitted signal is retained. The third factor-image (Fig. 5E–F, respectively) and the associated curve presents a negligible amount of radioactivity compared to the first two

factors. The magnitude of the associated radioactivity concentration is hundreds of times lower than the radioactivity of the first two factors.

Fig. 6 shows the result of the application of FA for cross-talk correction in one *in vivo* dual-radiotracer experiment ([ $^{123}\text{I}$ ]IBZM in Fig. 6A and [ $^{125}\text{I}$ ]R91150 in Fig. 6B) and the three factor curves (Fig. 6C). The images acquired *in vivo* correspond to the window between the 80th and the 110th minute post radiotracer injection for [ $^{123}\text{I}$ ]IBZM and between the 100th and the 120th minute post-injection for [ $^{125}\text{I}$ ]R91150. The corrected *in vivo* brain images present a predominant binding in striatum, compatible with the known spatial distribution of the [ $^{123}\text{I}$ ]IBZM. The spatial distribution of [ $^{125}\text{I}$ ]R91150 binding is as described in section 3.1. The third factor curve represents the rest of the radioactive signal that is negligible compared to the factor-images described above, as was the case for the phantom experiments. Both in the phantom and *in vivo* experiments, the two predominant factors have a visually similar spectral distribution pattern as the spectral patterns of energy emission extracted from single-radiotracer experiments (Fig. 2).

#### Correction of the cross-talk between $^{123}\text{I}$ and $^{125}\text{I}$ using the SRTM<sub>C</sub>

Fig. 7 shows the TACs extracted from a dynamic dual-radiotracer *in vivo* SPECT experiment using a VOI corresponding to the OFC (average of bilateral VOIs), a high 5-HT<sub>2A</sub> binding region. The TAC extracted from the image reconstructed at the high-energy spectrum is shown in red

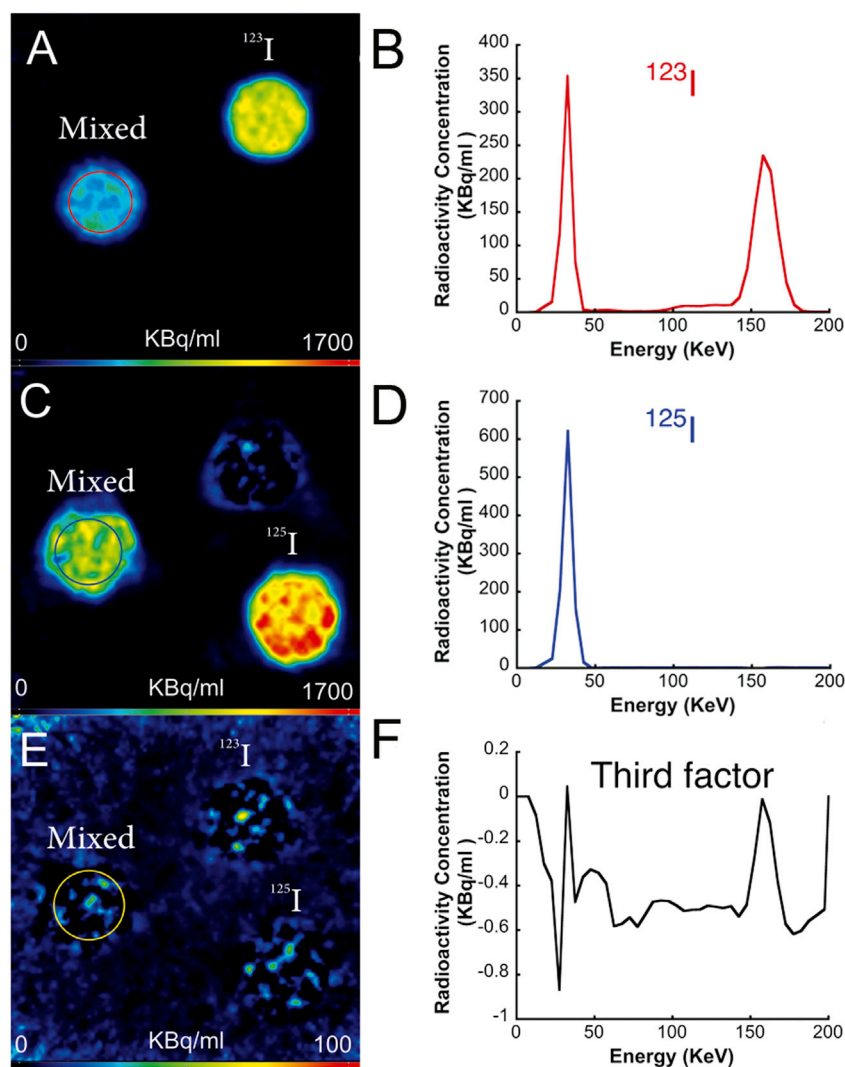


**Fig. 5.** Image-factors (A, C, E) and associated factor-curves (B, D, E) corresponding to  $^{123}\text{I}$ ,  $^{125}\text{I}$  and the third factor, obtained from FA application in phantom experiments. Note the minimal radioactivity attributed to the third factor (E and F) as opposed to the radioactivity from the first two factors.

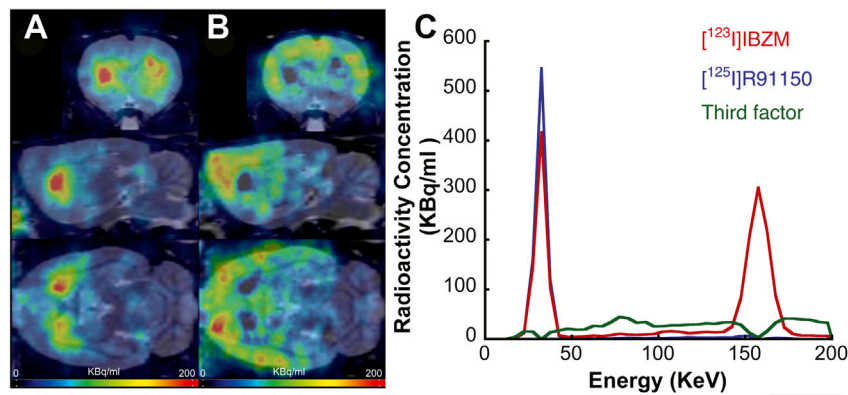


Fig. 6. Coronal, sagittal and axial planes of a FA-corrected *in vivo* [ $^{125}\text{I}$ ]R91150 (A) and [ $^{123}\text{I}$ ]IBZM (B) SPECT image. (C) the associated factor-curves.

color. This TAC corresponds to  $D_{2/3}$  binding and is unaffected by any cross-talk effect. In black color is the uncorrected TAC extracted from the image reconstructed at the low-energy spectrum. It is important to note that the initial part of the TAC (first 20 min) that corresponds to the scan duration before the injection of [ $^{123}\text{I}$ ]IBZM overlaps completely with the blue TAC, which is the corrected TAC with the SRTM<sub>C</sub> method. The injection of [ $^{123}\text{I}$ ]IBZM at the 20th minute induces a steep increase in the radioactive signal of [ $^{125}\text{I}$ ]R91150 and produces an important deviation from the normal kinetic pattern of this radiotracer. The SRTM<sub>C</sub> fitted the [ $^{125}\text{I}$ ]R91150-derived TACs in an excellent manner (data not shown). The  $\alpha'$  coefficient in CER, the reference region, was fixed at 0.34, the average value estimated in the series of rats that received only [ $^{123}\text{I}$ ]IBZM, as described in 2.5.1. The coefficient values for the brain VOIs, which were fitted with SRTM<sub>C</sub> had an average value of  $0.29 \pm 0.07$ , which was close to the average value of the  $\alpha$  coefficients estimated in the series of rats that received only [ $^{123}\text{I}$ ]IBZM, as described in 2.5.1.

#### Comparison of the methods for cross-talk correction

The radioactive concentrations obtained after cross-talk correction of the images of the phantoms containing both  $^{123}\text{I}$  and  $^{125}\text{I}$  were compared with the values obtained from the corresponding adjacent single-radioisotope containing tubes, which served as controls. For the DEW method, the linear regression for  $^{125}\text{I}$  provided an excellent correlation ( $r = 0.998$ ,  $p < 0.001$ , with a slope of the regression line of 0.96). Similarly, the  $^{125}\text{I}$  measurements after FA correction of cross-talk were excellent ( $r = 0.998$ ,  $p < 0.001$ , with a slope of 0.916). The  $^{123}\text{I}$  measurement after FA correction of cross-talk gave equally good results ( $r = 0.999$ ,  $p < 0.001$ , with a slope of 1.03).

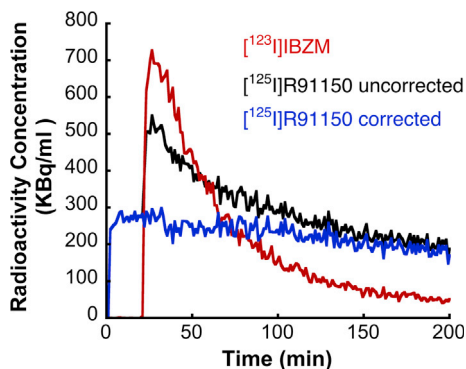


Fig. 7. TACs extracted from a dynamic dual-radiotracer *in vivo* SPECT experiment using a VOI corresponding to the OFC. The TAC extracted from the image reconstructed at the high-energy spectrum is shown in red color. In black color is the uncorrected TAC extracted from the image reconstructed at the low-energy spectrum. The blue TAC corresponds to the corrected [ $^{125}\text{I}$ ]R91150 TAC with the SRTM<sub>C</sub> method.

Table 2 presents BP<sub>ND</sub> values extracted from *in vivo* experiments. Examples of high- and low-binding VOIs for 5-HT<sub>2A</sub> (MC, MPFC, OFC) and  $D_{2/3}$  receptors (NAcc and CPu) are included. The SUR approach was applied over static dual-radiotracer images corrected with the DEW method and FA. The same approach was applied to single-radiotracer SPECT images for comparison. BP<sub>ND</sub> values extracted from dynamic dual-radiotracer images using the cross-talk correction in the SRTM<sub>C</sub> are also included. BP<sub>ND</sub> values from frontal cortical regions estimated from DEW-corrected dual-radiotracer images ranged from  $3.86 \pm 0.24$  in the MC to  $4.75 \pm 0.96$  in the OFC. FA-corrected images provided similar values ranging from  $3.77 \pm 0.29$  to  $4.77 \pm 0.93$ , respectively. SRTM<sub>C</sub>-derived BP<sub>ND</sub> values were found in a similar range, i.e. from  $3.78 \pm 0.11$  in the MC to  $5.18 \pm 1.73$  in the OFC. Regarding the high-5-HT<sub>2A</sub> binding VOIs, all correction methods provide overestimated values, compared to values estimated using the same methods from single-radiotracer experiments and in the case of the DEW- and FA-derived BP<sub>ND</sub> values reached statistical significance (as evaluated by means of paired-samples *t*-test). The extraction of [ $^{123}\text{I}$ ]IBZM images from dual-radiotracer experiments using FA provides average BP<sub>ND</sub> values which are very close to the values estimated from [ $^{123}\text{I}$ ]IBZM images that were directly reconstructed at the high energy window (shown in the last column of Table 2).

Furthermore, an evaluation of the cross-talk correction methods was performed. BP<sub>ND</sub> estimations from the dual-radiotracer experiments, corrected with each one of the three methods were compared to the estimations from single-radiotracer [ $^{123}\text{I}$ ]R91150 experiments by means of linear regression analysis. BP<sub>ND</sub> values were averaged in every VOI across the rats of the same group and regression analysis was performed using average these VOI values. Average BP<sub>ND</sub> values estimated in cross-talk corrected [ $^{125}\text{I}$ ]R91150 images using the DEW method correlated well with average BP<sub>ND</sub> values from single-radiotracer [ $^{123}\text{I}$ ]R91150 experiments ( $r = 0.92$ ,  $p < 0.001$ , Fig. 8A). Similarly, BP<sub>ND</sub> values from [ $^{125}\text{I}$ ]R91150 images corrected with FA correlated equally well ( $r = 0.92$ ,  $p < 0.001$ , Fig. 8B). BP<sub>ND</sub> values from the spectral FA-extracted [ $^{123}\text{I}$ ]IBZM images from dual-radiotracer experiments were compared to BP<sub>ND</sub> values from the exact same images that were reconstructed at the high-energy spectrum, where only unbiased  $^{123}\text{I}$ -emitted radioactivity is detected ( $r = 0.99$ ,  $p < 0.001$ , Fig. 8C). A similar same level of agreement was observed using the SRTM<sub>C</sub> to account for the impact of cross-talk on [ $^{125}\text{I}$ ]R91150 kinetics ( $r = 0.92$ ,  $p < 0.001$ , Fig. 8D).

#### Evaluation of the relationship between striatal $D_{2/3}$ and 5-HT<sub>2A</sub>-receptor binding at the voxel and VOI level

Fig. 9 A presents a coronal section of a parametric image of Pearson's *r* coefficients. Linear regression analysis was performed to compare  $D_{2/3}$  and 5-HT<sub>2A</sub> binding across the six rats of the experiment at the voxel level. Parametric images of associated *p* values of statistical significance reveal that two small clusters of voxels (<20 voxels) in each NAcc reach

**Table 2**  
BP<sub>ND</sub> (ml/ml) values extracted from dual- and single-radiotracer studies. Values are presented as mean ± standard deviation. The unbiased (control) values were obtained from a single-radiotracer [<sup>123</sup>I]R91150 experiment (4 rats) while the unbiased [<sup>123</sup>I]IBZM values were obtained after the reconstruction of the images of the dual-radiotracer experiments at the high energy window, which is not affected by any cross-talk. No BP<sub>ND</sub> values outside the striatum are presented for [<sup>123</sup>I]IBZM.

VOI	Dual radiotracer-experiments				Unbiased (control) experiments	
	[ <sup>125</sup> I]R91150			[ <sup>123</sup> I]IBZM	[ <sup>123</sup> I]R91150	[ <sup>123</sup> I]IBZM
	DEW (SUR)	FA (SUR)	SRTM <sub>C</sub>	FA (SUR)	SUR	SUR
MC	3.86 ± 0.24	3.77 ± 0.29	3.78 ± 0.11	–	2.85 ± 0.21	–
MPFC	4.20 ± 1.13	4.76 ± 0.87	4.28 ± 0.74	–	3.48 ± 0.48	–
OFC	4.75 ± 0.96	4.77 ± 0.93	5.18 ± 1.73	–	3.34 ± 0.24	–
NAcc	1.94 ± 0.66	2.26 ± 0.64	2.04 ± 0.45	2.61 ± 0.29	2.55 ± 0.43	2.59 ± 0.6
CPu	2.51 ± 0.54	2.66 ± 0.57	2.94 ± 0.42	5.12 ± 0.59	2.53 ± 0.34	4.93 ± 0.92

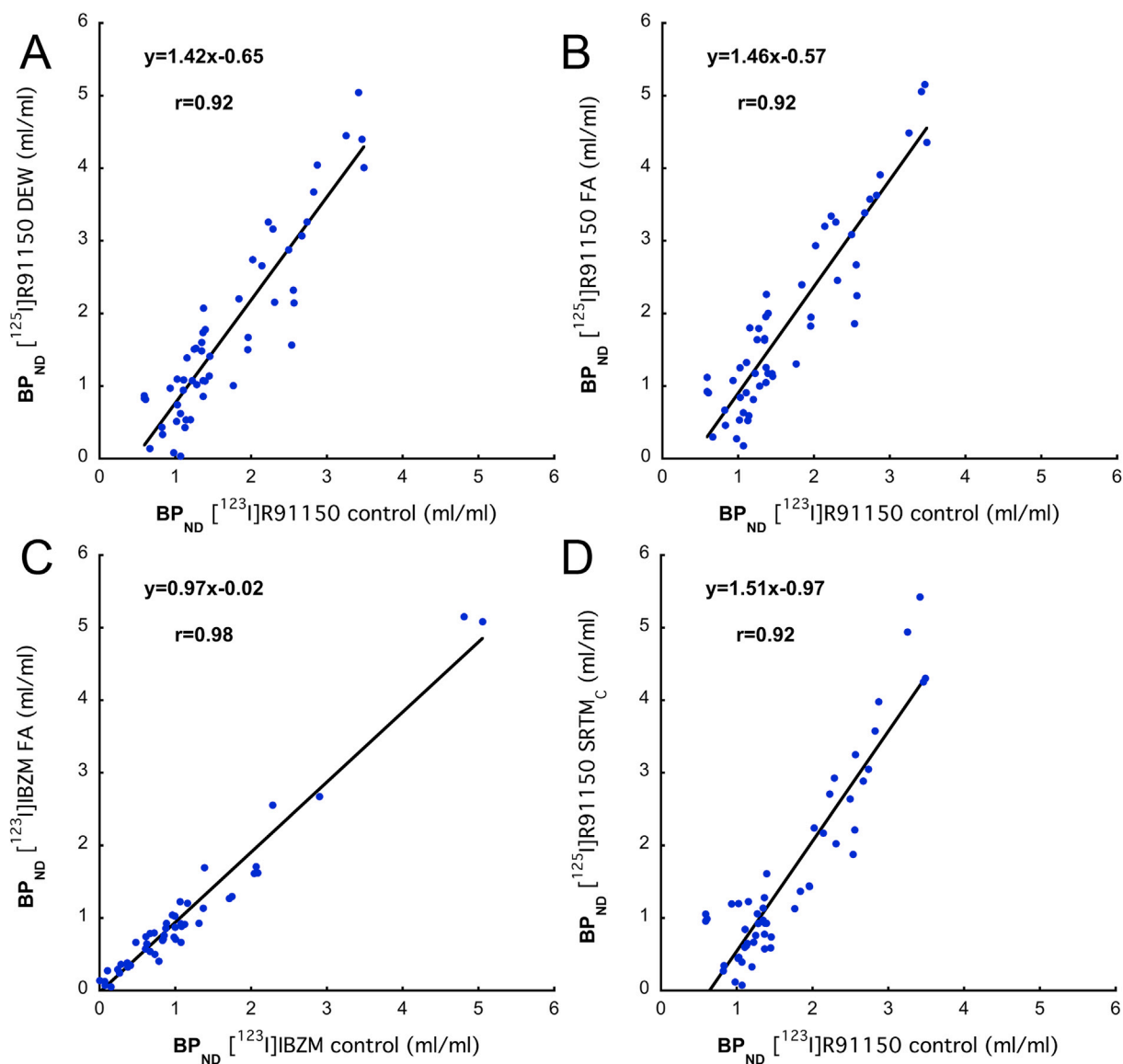


**Fig. 8.** Scatterplot of average (across rats) regional [<sup>125</sup>I]R91150 BP<sub>ND</sub> values (vertical axis) from the dual-radiotracer *in vivo* experiments corrected with the (A) DEW (Method 1) and (B) spectral FA (Method 2). They are plotted against average [<sup>123</sup>I]R91150 BP<sub>ND</sub> values from the single-radiotracer experiments (horizontal axis). (C) Correlation between average [<sup>123</sup>I]IBZM BP<sub>ND</sub> values obtained after the application of FA (vertical axis) and the average BP<sub>ND</sub> values from the direct reconstruction of [<sup>123</sup>I]IBZM at the high-energy spectrum (which is unbiased) from the same experiments (horizontal axis). SRTM<sub>C</sub> (Method 3). (D) Scatterplot of average [<sup>125</sup>I]R91150 BP<sub>ND</sub> values (vertical axis) obtained with the SRTM<sub>C</sub> method plotted against the average [<sup>123</sup>I]R91150 BP<sub>ND</sub> values from the single-radiotracer experiments (horizontal axis).

significance at  $p < 0.05$ . Linear regression analysis was also performed for the comparison of  $D_{2/3}$  and 5-HT<sub>2A</sub> binding across these six rats at the VOI level in bilateral CPu and NAcc. A statistically significant correlation is observed ( $r = 0.78$ ,  $p < 0.01$ , Fig. 9B) in NAcc, but not in CPu (data not shown).

## Discussion

### *BP<sub>ND</sub> estimation from dual-radiotracer SPECT studies*

The present paper evaluates three different methods for the simultaneous, dual-radiotracer imaging using a <sup>123</sup>I- and a <sup>125</sup>I-labeled molecule. These methods correct the effect of cross-talk on radioactivity measurements of <sup>125</sup>I. All three methods provide BP<sub>ND</sub> values of [<sup>125</sup>I]R91150 that correlate highly with values obtained from single-radiotracer [<sup>123</sup>I]R91150 experiments and are similar to values from the literature (Dumas et al., 2015; Tsartsalis et al., 2016b, 2017). Using one of the proposed methods (DEW), we also demonstrated that BP<sub>ND</sub> values from dual-radiotracer experiments have an acceptable test-retest variability, which is 14% for [<sup>123</sup>I]IBZM and 14.10% for [<sup>125</sup>I]R91150 (see section S2.1). Indeed, in SPECT, [<sup>123</sup>I]R91150 BP<sub>ND</sub> values' test-retest variability ranges between 10 and 20% (Catafau et al., 2008). In small animal imaging in general, a variability of 15–20% is considered acceptable (Constantinescu et al., 2011), as is the case for the BP<sub>ND</sub> values presented here.

The DEW method (Method 1) provides the most straightforward means of correction of the cross-talk between <sup>123</sup>I- and <sup>125</sup>I-labeled molecules. It exploits the linear relationship between the <sup>123</sup>I-emitted activity on the <sup>125</sup>I spectrum and thus its use has no statistical noise. To our knowledge, the present paper is the first to employ this method in brain imaging (Lee et al., 2013, 2015). The validity of this method is supported by the excellent correlation between BP<sub>ND</sub> values from DEW-corrected, dual-radiotracer and from single-radiotracer SPECT studies. One disadvantage of this method is the variability of the  $\alpha$  coefficient values across the brain regions, due to the interaction of photons with matter. Indeed, this interaction is illustrated by the difference in the value of the  $\alpha$  coefficient as estimated in phantoms (where there is a minimal interaction with matter) and *in vivo*. This is not surprising and has been described for another pair of SPECT-employed radioisotopes, <sup>111</sup>In/<sup>111</sup>In and <sup>177</sup>Lu (Hijnen et al., 2012). Importantly, in our experiments, the effect of the interaction with matter is quite homogeneous across the brain VOI and across rats with a coefficient of variation of  $\alpha$  at 17%. This variation in the  $\alpha$  parameter values, albeit non-negligible *per se*, probably has a little impact in the context of this study. Indeed, looking into the value of this parameter in individual VOI across rats shows that in cortical, receptor-rich regions, as well as in the striatum and the CER,  $\alpha$  values are less variable (with a coefficient of variation  $< 10\%$  as described in section 3.1 and close to the average value that was used in the application of the DEW method).

Using FA (Method 2) for the correction of the cross-talk resulted in BP<sub>ND</sub> values that correlated similarly well with the [<sup>123</sup>I]R91150 values from the single-radiotracer group. As a further validation step, the BP<sub>ND</sub> values of [<sup>123</sup>I]IBZM extracted with FA was directly compared to the corresponding values from [<sup>123</sup>I]IBZM images that were directly reconstructed at the principal (hence cross-talk-free) emission spectrum of <sup>123</sup>I. The highly significant correlation proposes that FA does not considerably bias the radioactivity measurements. The use of extra-striatal BP<sub>ND</sub> values in the linear regression analysis of <sup>123</sup>I binding may appear odd, given the lack of specific binding of [<sup>123</sup>I]IBZM out of the striatum. However, the objective of this comparison was to assess the correction of a physical phenomenon (cross-talk) that is little affected, if at all, by the kind of binding (specific, free or non-specific). The application of FA is not limited to dual <sup>123</sup>I and <sup>125</sup>I experiments but extends to dual <sup>123</sup>I and <sup>99m</sup>Tc imaging, which may equally be applied in clinical neuroimaging. Indeed, correction of cross-talk between <sup>123</sup>I and <sup>99m</sup>Tc with independent component analysis has been described in the literature (Chang et al.,

2006). In the same paper, this method proved superior to a simple reconstruction using an energy spectrum at 15% around the <sup>99m</sup>Tc photopeak. Model-based correction methods have also been proposed for this correction (Du and Frey, 2009; El Fakhri et al., 2001). Another advantage of FA is that it may potentially be used for triple-radiotracer SPECT using <sup>123</sup>I, <sup>125</sup>I and <sup>99m</sup>Tc and preliminary studies of our group on phantoms show promising results (data not shown). FA is not as straightforward as the DEW method and presents a statistical noise. In addition, in voxels that have the highest binding of the <sup>123</sup>I-labeled radiotracer and a moderate or low binding of the <sup>125</sup>I-labeled radiotracer, FA tends to attribute all the radioactivity to the <sup>123</sup>I, thus underestimate the <sup>125</sup>I-associated binding. This seems to be the case for some striatal voxels, as illustrated in Fig. 6B. This could be of little importance when BP<sub>ND</sub> values are studied in whole VOIs but could be a considerable limitation in voxel-wise quantification.

Method 3, which implements the cross-talk correction in the kinetic analysis with SRTM, provides a valuable alternative to the previous two methods when kinetic modeling in dynamic images is required for quantification. Indeed, using the first two methods, FA in particular, in dynamic studies would be computationally challenging. One disadvantage of the SRTM<sub>C</sub> method is the need for an interval between the injections of each radiotracer. In addition, SRTM<sub>C</sub> necessitates an *a priori* determination of the  $\alpha$  coefficient in the reference region to optimize the identifiability of the model's parameters. Nevertheless, an interesting finding is that the estimates of the  $\alpha$  coefficient with Method 3 have comparable values to the ones found with Method 1 and this consistency is, to our view, an argument in favor of the validity of the proposed methods.

Given the fact that Method 1 (DEW) is the most straightforward and computationally feasible to apply, while it has no statistical noise, it was the method of choice for the study of the relationship of  $D_{2/3}$  and 5-HT<sub>2A</sub> receptor binding in the striatum, as discussed further in this paper.

### *Dual-radiotracer imaging in PET and SPECT*

Dual SPECT imaging is feasible when radiotracers are labeled with radioisotopes with non-overlapping emission spectra (Akutsu et al., 2009; Antunes et al., 1992; Bruce et al., 2000; Ichihara et al., 1993). Dual [<sup>99m</sup>Tc]pyrophosphate/<sup>201</sup>Tl SPECT has been proposed in cardiac nuclear imaging to assess the viability of the myocardium and its irrigation, respectively. Similarly, <sup>201</sup>Tl/<sup>123</sup>Iβ-methyl-iodophenyl pentadecanoic acid (BMIPP) dual-radiotracer SPECT has been described for a simultaneous assessment of cardiac perfusion (<sup>201</sup>Tl) and fatty acid metabolism ([<sup>123</sup>I]BMIPP) (Akutsu et al., 2004). In both cases, the energy emission spectra of the combined radioisotopes had no considerable overlap, thus no cross-talk correction was required. <sup>111</sup>In/<sup>177</sup>Lu dual-radioisotope SPECT has also been described, given the minimal overlap of their respective emission spectra, with a DEW method to account for this overlap (Hijnen et al., 2012).

Recently, a PET system that proposes dual (or higher) simultaneous radiotracer imaging using pure positron and positron-γ emitters, has been described (Fukuchi et al., 2017). In addition, discrimination of positron-emitting radioisotopes based on their unique decay rate has been described for <sup>18</sup>F and <sup>13</sup>N (Figueiras et al., 2011). Dual-radiotracer PET has also been described in the case of brain tumor studies in which tumor metabolism and proliferative activity are assessed with [<sup>18</sup>F]FDG and [<sup>18</sup>F]FLT, respectively. In that paper, a joint-radiotracer pharmacokinetic model was considered and all the kinetic parameters were estimated from a PET dynamic study in which the two radiotracers were injected with a 30-min delay from each other (Kadmas et al., 2013). A longer delay between the two radiotracers' injections may be appropriate when short half-life radiotracers are used (Koepe et al., 2001). Overall, our study is the first among the aforementioned ones which proposes a dual-radiotracer imaging methodology with radioiodinated molecules in the brain and a direct biological application.

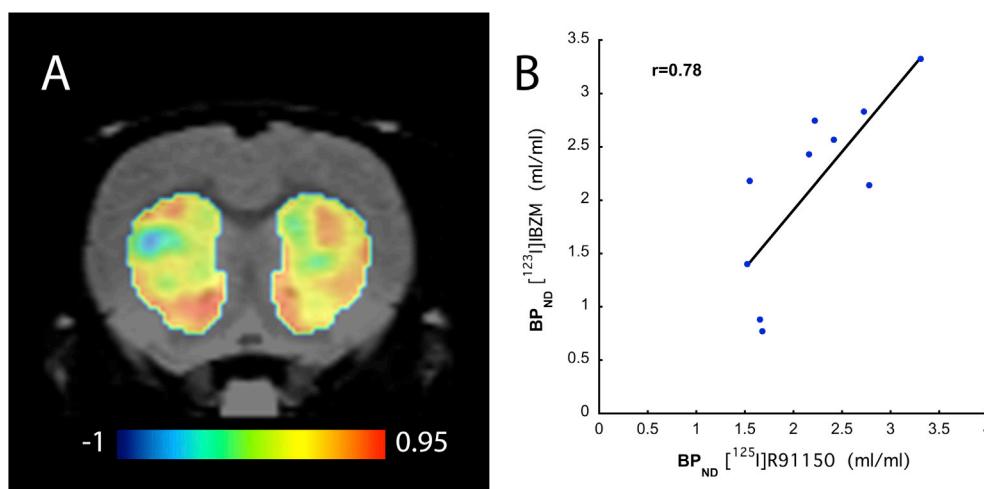


**Fig. 9.** (A) a coronal section of a parametric image of Pearson's  $r$  coefficients. Linear regression analysis was performed to compare  $D_{2/3}$  and 5-HT $_{2A}$  binding across the six rats of the experiment at the voxel level. The color bar represents  $r$  values. (B) Linear regression analysis for the comparison of  $D_{2/3}$  and 5-HT $_{2A}$  binding across ten rats at the VOI level (including average left and right NAcc for each rat).

#### Simultaneous study of $D_{2/3}$ and 5-HT $_{2A}$ binding in the striatum

The *in vivo* study of multiple receptors or proteins in general, is an approach of great potential, as the understanding of brain physiology and pathology may not be limited to the study of one molecular target. In the present study, to emphasize on the feasibility of performing simultaneous, dual-radiotracer SPECT studies *in vivo*, we provide preliminary evidence for an association of  $D_{2/3}$  and 5-HT $_{2A}$  receptors in the NAcc. We employed Method 1 (DEW) to study the relationship between  $D_{2/3}$  and 5-HT $_{2A}$  binding because it is the most straightforward.  $D_{2/3}$  and 5-HT $_{2A}$  BP<sub>ND</sub> values show a positive correlation, at the VOI level, in NAcc. In a preliminary evaluation of the same relationship at the voxel level, we find that  $D_{2/3}$  and 5-HT $_{2A}$  binding showed a good correlation in the NAcc across the rats. Given the fact that this is an exploratory analysis, with a primary purpose to validate the dual-radioligand approach (which is intended to use with any couple of molecular targets in the brain and not limited to  $D_{2/3}$  and 5-HT $_{2A}$ ), with a limited number of rats and without any correction for the effects of noise, we did not perform any correction for multiple comparisons. In this context, formulating conclusions on the biological underpinnings of this voxel-wise correlation is out of the scope of this paper.

Evidently, one could hypothesize that there is no real correlation and that [ $^{123}$ I]IBZM contaminates [ $^{125}$ I]R91150 radioactivity measurements due to suboptimal correction of cross-talk. The simulation study described in section S2.3 shows that even in the “worst-case” scenario where both striatal and cerebellar  $\alpha$  coefficient values have been miscalculated (by 20% that exceeds the variability of  $\alpha$  coefficient estimates from [ $^{123}$ I]IBZM-only experiments as estimated in 2.5.1), the change of the slope of the regression line does not produce an artificial correlation. As a further proof, we performed the analysis in S2.3, in which radiolabeling with  $^{123}$ I and  $^{125}$ I was inverted for IBZM and R91150. In this case we evaluate the scenario where  $^{123}$ I radioactivity in high [ $^{123}$ I]R91150-binding VOIs (such as in cortical VOIs) highly contaminates the signal from [ $^{125}$ I]IBZM which is virtually inexistent in the same regions. Knowing that no specific binding of [ $^{125}$ I]IBZM is observed out of the striatum, we safely assume that no correlation should be observed after the correction for cross-talk whatsoever. Before correction, voxel-wise BP<sub>ND</sub> values between the two radiotracers correlated well (data not shown). This is not surprising, given the high level of  $^{123}$ I-derived radioactivity that is measured at the  $^{125}$ I energy spectrum. After correction for cross-talk, no voxel-wise correlation at any of the VOIs was observed, thus further confirming the validity of the DEW method that demonstrated this correlation between the two receptors. We also rule

out the possibility that the observed correlation is in fact biased by the partial volume effects on [ $^{125}$ I]R91150 binding in NAcc from adjacent high-binding cortical VOIs. Indeed, no correlations are observed between  $D_{2/3}$  binding in NAcc and 5-HT $_{2A}$  binding in either of these cortical regions (S2.3). In addition, our *in vitro* autoradiography study (see Supplemental S1.4), shows that in NAcc, regional  $D_{2/3}$  binding correlates with 5-HT $_{2A}$  binding, further supporting the *in vivo* study.

Evidence in the literature on  $D_2$  and 5-HT $_{2A}$  interactions already exists: they may be co-expressed on the same cells (Ma et al., 2006) or form functional heterodimers (Albizu et al., 2011; Borroto-Escuela et al., 2014; Lukaszewicz et al., 2010) in physiological or pathological conditions (Varela et al., 2015). Nonetheless, the full extent of the biological implications of such an interaction remains elusive. In this context, dual-radiotracer imaging of  $D_{2/3}$  and 5-HT $_{2A}$  (as well as of other couples of molecular targets) may constitute a complementary means for the non-invasive, *in vivo* study of such complex biological phenomena.

#### Limitations

Our study has three main limitations. First, performing single- and dual-radiotracer experiments on the same rat at different time-points could provide a better comparison group for the validation of the methods proposed for the correction of cross-talk between  $^{123}$ I and  $^{125}$ I and further validation of the results with this approach is encouraged, especially if other couples of radiotracers are employed in future experiments. Indeed, averaging values across rats before comparison may diminish the effect of BP<sub>ND</sub> variability. Nevertheless, we chose to use three independent groups of rats instead of using the same group and multiple scans for each animal to minimize stress for the animals. In addition, the use of the same rat at different time-points would still be subject to the test-retest variability. The scanning protocol employed in the study was quite long and this constituted a technical difficulty for using the same rats twice. Despite this limitation, the linear regression analysis results demonstrate a highly significant correlation between [ $^{125}$ I]R91150 values from dual-radiotracer and [ $^{123}$ I]R91150 values from single-radiotracer experiments.

Another limitation concerns the observed correlation between NAcc [ $^{123}$ I]IBZM and [ $^{125}$ I]R91150 BP<sub>ND</sub> values. Despite support from literature, there is no direct study of the biological implications of this finding. However, this would be largely out of the scope of this paper, which intends to illustrate that using dual-radiotracer SPECT in translational research may reveal such relationships between different aspects of a biological phenomenon, to permit an *in vivo* longitudinal assessment and,

finally, to be coupled with studies at the cellular and molecular level. Furthermore, in the present paper, no assessment of this relationship in extra-striatal regions may be obtained given the absence of specific binding of [ $^{123}\text{I}$ ]IBZM in these regions. Such a study may be performed with [ $^{123}\text{I}$ ]epidepride, a high-affinity  $\text{D}_{2/3}$  radiotracer presenting specific binding in extra-striatal regions. Our proposed methods may be directly applied in a dual-radiotracer [ $^{123}\text{I}$ ]epidepride/[ $^{125}\text{I}$ ]R91150 study, as with any couple of radio-iodinated molecules.

Finally, we did not perform either scatter or attenuation correction in our *in vivo* imaging studies. Both corrections should be important (Andersen et al., 2014), particularly with the DEW method (Lee et al., 2015).  $^{125}\text{I}$ , in particular, is more subject to attenuation and scatter effects than  $^{123}\text{I}$  (Feng et al., 2007; Gregor et al., 2007). Correcting for the effects of these phenomena should diminish the bias presented in  $\text{BP}_{\text{ND}}$  values of [ $^{125}\text{I}$ ]R91150 compared to [ $^{123}\text{I}$ ]R91150, which is evident from Fig. 8 and Table 2. In fact, despite excellent correlations,  $\text{BP}_{\text{ND}}$  values from dual-radiotracer experiments were overestimated with all three correction methods (with the values of the DEW and FA methods reaching statistically significant difference from [ $^{123}\text{I}$ ]R91150  $\text{BP}_{\text{ND}}$  values). This overestimation is, at least in its greatest part, the result of the effects of scatter and attenuation on  $^{125}\text{I}$  imaging *per se* and not of any bias in the dual-radiotracer imaging approaches described here. As shown in supplemental Fig. S2, [ $^{125}\text{I}$ ]R91150  $\text{BP}_{\text{ND}}$  values from dual-radiotracer experiments correlate well with [ $^{125}\text{I}$ ]R91150  $\text{BP}_{\text{ND}}$  values from single-radiotracer experiments and do not differ significantly from them. Thus, it may be hypothesized that the origin of this overestimation, affecting both single- and dual-radiotracer studies with [ $^{125}\text{I}$ ]R91150 is probably due to the aforementioned physical phenomena and a more pronounced effect of them on the radioactivity in reference region (CER) that in target VOI in the rat brain. As it may be observed in Fig. S5, VOI situated on the basis of the skull (i.e. those highlighted in red on the scatter plot) are less overestimated compared to [ $^{123}\text{I}$ ]R91150  $\text{BP}_{\text{ND}}$  values than the other, more superficial regions. This is probably due to a more pronounced effect of scatter and attenuation in these VOI. However, without CT data from our experiments, attenuation correction could not be performed. Regarding scatter correction, we performed a preliminary correction with DEW on the three rats of the dual radiotracer validation study (experiment 3 in Table 1) after having corrected data for scatter with the triple-energy window (TEW). This resulted in  $\text{BP}_{\text{ND}}$  values which correlated in an excellent manner with the corresponding  $\text{BP}_{\text{ND}}$  values from studies uncorrected for scatter. Given this result, the fact that scatter correction may be time-consuming and that scatter correction alone without attenuation correction may add further bias (Hutton et al., 2011), we chose not to implement scatter correction in our DEW methodology. In any case, our proposed methods may be substantially optimized with the correction of the scatter and attenuation effects (Lee et al., 2015), which was out of the scope of this paper.

## Conclusion

Dual- and potentially multiple-radiotracer imaging may prove to be an invaluable tool in molecular imaging with both PET and SPECT. Numerous studies in neuropsychiatry already employ multiple-radiotracer imaging. Here, we provide three different methods for the correction of cross-talk produced by the overlap between the emission spectra of  $^{123}\text{I}$  and  $^{125}\text{I}$ . Among these methods, the DEW method is considered the most straightforward and computationally feasible. This applicability of this method was demonstrated in an experiment that showed that  $\text{NAcc}_{\text{D}_{2/3}}$  and  $5\text{-HT}_{2\text{A}}$  binding are correlated at the voxel and VOI level.

## Acknowledgments

This work was supported by the Swiss National Science Foundation (grant no. 310030\_156829), by the Geneva Neuroscience Center and by the Maria Zausi Memorial Foundation (Greece) through a scholarship of

the Hellenic State Scholarship Foundation (ST) and by the “Swiss Association for Alzheimer's Research” which was created in 2009 to finance Swiss fundamental and clinical research programs on Alzheimer's disease. Dr Vallez-Garcia of the University Medical Center Groningen (UMCG) provided valuable expertise regarding the SAMIT Toolbox. Authors are grateful to Mrs Maria Surini-Demiri and Mr Marouane Ben Ammar for excellent technical assistance and declare that they have no conflict of interest.

## Appendix A. Supplementary data

Supplementary data related to this article can be found at <https://doi.org/10.1016/j.neuroimage.2018.04.063>.

## References

- Akutsu, Y., Kaneko, K., Kodama, Y., Li, H.L., Nishimura, H., Hamazaki, Y., Suyama, J., Shinozuka, A., Gokan, T., Kobayashi, Y., 2009. Technetium-99m pyrophosphate/thallium-201 dual-isotope SPECT imaging predicts reperfusion injury in patients with acute myocardial infarction after reperfusion. *Eur. J. Nucl. Med. Mol. Imaging* 36, 230–236.
- Akutsu, Y., Shinozuka, A., Kodama, Y., Li, H.L., Kayano, H., Hamazaki, Y., Yamanaka, H., Katagiri, T., 2004. Usefulness of simultaneous evaluations of contractile reserve, perfusion, and metabolism during dobutamine stress for predicting wall motion reversibility (myocardial stunning) after successful PTCA. *Jpn. Heart J.* 45, 195–204.
- Albizu, L., Holloway, T., Gonzalez-Maeso, J., Sealfon, S.C., 2011. Functional crosstalk and heteromerization of serotonin 5-HT<sub>2A</sub> and dopamine D<sub>2</sub> receptors. *Neuropharmacology* 61, 770–777.
- Andersen, F.L., Ladefoged, C.N., Beyer, T., Keller, S.H., Hansen, A.E., Hojgaard, L., Kjaer, A., Law, I., Holm, S., 2014. Combined PET/MR imaging in neurology: MR-based attenuation correction implies a strong spatial bias when ignoring bone. *Neuroimage* 84, 206–216.
- Antunes, M.L., Johnson, L.L., Seldin, D.W., Bhatia, K., Tresgallo, M.E., Greenspan, R.L., Vaccarino, R.A., Rodney, R.A., 1992. Diagnosis of right ventricular acute myocardial infarction by dual isotope thallium-201 and indium-111 antimony SPECT imaging. *Am. J. Cardiol.* 70, 426–431.
- Baeken, C., D'Haenen, H., Flamen, P., Mertens, J., Terriere, D., Chavatte, K., Boumon, R., Bossuyt, A., 1998. 123I-5-I-R91150, a new single-photon emission tomography ligand for 5-HT<sub>2A</sub> receptors: influence of age and gender in healthy subjects. *Eur. J. Nucl. Med.* 25, 1617–1622.
- Boroto-Escuela, D.O., Romero-Fernandez, W., Narvaez, M., Oflijan, J., Agnati, L.F., Fuxe, K., 2014. Hallucinogenic 5-HT<sub>2A</sub> agonists LSD and DOI enhance dopamine D<sub>2R</sub> promoter recognition and signaling of D<sub>2</sub>-5-HT<sub>2A</sub> heteroreceptor complexes. *Biochem. Biophys. Res. Commun.* 443, 278–284.
- Bruce, I.N., Burns, R.J., Gladman, D.D., Urowitz, M.B., 2000. Single photon emission computed tomography dual isotope myocardial perfusion imaging in women with systemic lupus erythematosus. I. Prevalence and distribution of abnormalities. *J. Rheumatol.* 27, 2372–2377.
- Carson, R.E., Wu, Y., Lang, L., Ma, Y., Der, M.G., Herscovitch, P., Eckelman, W.C., 2003. Brain uptake of the acid metabolites of F-18-labeled WAY 100635 analogs. *J. Cereb. Blood Flow. Metab.* 23, 249–260.
- Catafau, A.M., Bullich, S., Danus, M., Penengo, M.M., Cot, A., Abanades, S., Farre, M., Pavia, J., Ros, D., 2008. Test-retest variability and reliability of 123I-IBZM SPECT measurement of striatal dopamine D<sub>2</sub> receptor availability in healthy volunteers and influence of iterative reconstruction algorithms. *Synapse* 62, 62–69.
- Chang, C., Huang, W., Su, H., Chen, J., 2006. Separation of two radionuclides in simultaneous dual-isotope imaging with independent component analysis. *Biomed. Eng. Appl. Basis Comm.* 18, 264–269.
- Constantinescu, C.C., Coleman, R.A., Pan, M.L., Mukherjee, J., 2011. Striatal and extra-striatal microPET imaging of D<sub>2</sub>/D<sub>3</sub> dopamine receptors in rat brain with [(1)(8)F]fallypride and [(1)(8)F]desmethoxyfallypride. *Synapse* 65, 778–787.
- Cselenyi, Z., Lundberg, J., Halldin, C., Farde, L., Gulyas, B., 2004. Joint explorative analysis of neuroreceptor subsystems in the human brain: application to receptor-transporter correlation using PET data. *Neurochem. Int.* 45, 773–781.
- Cunha, L., Horvath, I., Ferreira, S., Lemos, J., Costa, P., Vieira, D., Veres, D.S., Szigeti, K., Summavielle, T., Mathe, D., Metello, L.F., 2014. Preclinical imaging: an essential ally in modern biosciences. *Mol. Diagn. Ther.* 18, 153–173.
- De Bruyne, S., Wyffels, L., Boos, T.L., Staelens, S., Deleze, S., Rice, K.C., De Vos, F., 2010. In vivo evaluation of [123I]-4-(2-(bis(4-fluorophenyl)methoxy)ethyl)-1-(4-iodobenzyl)piperidine, an iodinated SPECT tracer for imaging the P-gp transporter. *Nucl. Med. Biol.* 37, 469–477.
- Di Paola, R., Bazin, J.P., Aubry, F., Aurengo, A., Cavailloles, F., Herry, J.Y., Kahn, E., 1982. Handling of dynamic sequences in nuclear medicine. *IEEE Trans Nucl. Sci. N. S.* 29, 1310–1321.
- Du, Y., Frey, E.C., 2009. Quantitative evaluation of simultaneous reconstruction with model-based crosstalk compensation for 99mTc/123I dual-isotope simultaneous acquisition brain SPECT. *Med. Phys.* 36, 2021–2033.
- Dumas, N., Moulin-Sallanon, M., Fender, P., Tournier, B.B., Ginovart, N., Charnay, Y., Millet, P., 2015. In vivo quantification of 5-HT<sub>2A</sub> brain receptors in Mdr1a KO rats with 123I-R91150 single-photon emission computed tomography. *Mol. Imaging* 14.

- Dumas, N., Moulin-Sallanon, M., Ginovart, N., Tournier, B.B., Suzanne, P., Cailly, T., Fabis, F., Rault, S., Charnay, Y., Millet, P., 2014. Small-animal single-photon emission computed tomographic imaging of the brain serotonergic systems in wild-type and *mdr1a* knockout rats. *Mol. Imaging* 13.
- El Fakhri, G., Moore, S.C., Maksud, P., Aurengo, A., Kijewski, M.F., 2001. Absolute activity quantitation in simultaneous  $^{123}\text{I}/^{99\text{m}}\text{Tc}$  brain SPECT. *J. Nucl. Med.* 42, 300–308.
- Fakhri, G.E., 2012. Ready for prime time? Dual tracer PET and SPECT imaging. *Am. J. Nucl. Med. Mol. Imaging* 2, 415–417.
- Feng, B., Bai, B., Smith, A.M., Austin, D.W., Mintzer, R.A., Gregor, J., 2007. Reconstruction of multi-pinhole SPECT data with correction of attenuation, scatter and intrinsic detector resolution. In: 2007 IEEE Nuclear Science Symposium Conference Record, pp. 3482–3485.
- Figueiras, F.P., Jimenez, X., Pareto, D., Gomez, V., Llop, J., Herance, R., Rojas, S., Gispert, J.D., 2011. Simultaneous dual-tracer PET imaging of the rat brain and its application in the study of cerebral ischemia. *Mol. Imaging Biol.* 13, 500–510.
- Frankle, W.G., Laruelle, M., 2002. Neuroreceptor imaging in psychiatric disorders. *Ann. Nucl. Med.* 16, 437–446.
- Frankle, W.G., Slifstein, M., Talbot, P.S., Laruelle, M., 2005. Neuroreceptor imaging in psychiatry: theory and applications. *Int. Rev. Neurobiol.* 67, 385–440.
- Fukuchi, T., Okauchi, T., Shigeta, M., Yamamoto, S., Watanabe, Y., Enomoto, S., 2017. Positron emission tomography with additional gamma-ray detectors for multiple-tracer imaging. *Med. Phys.*
- Ginovart, N., Kapur, S., 2012. Role of dopamine D(2) receptors for antipsychotic activity. *Handb. Exp. Pharmacol.* 27–52.
- Gregor, J., Black, N., Wall, J., 2007. Monte Carlo study of scatter and attenuation effects in connection with I-125 pinhole imaging of mice. In: International Meeting on Fully 3D Image Reconstruction in Radiology and Nuclear Medicine (Lindau, Germany).
- Hijnen, N.M., de Vries, A., Nicolay, K., Grull, H., 2012. Dual-isotope  $^{111}\text{In}/^{177}\text{Lu}$  SPECT imaging as a tool in molecular imaging tracer design. *Contrast Media Mol. Imaging* 7, 214–222.
- Howes, O.D., Kambeitz, J., Kim, E., Stahl, D., Slifstein, M., Abi-Dargham, A., Kapur, S., 2012. The nature of dopamine dysfunction in schizophrenia and what this means for treatment. *Arch. Gen. Psychiatry* 69, 776–786.
- Hutton, B.F., Buvat, I., Beekman, F.J., 2011. Review and current status of SPECT scatter correction. *Phys. Med. Biol.* 56, R85–R112.
- Ichihara, T., Ogawa, K., Motomura, N., Kubo, A., Hashimoto, S., 1993. Compton scatter compensation using the triple-energy window method for single- and dual-isotope SPECT. *J. Nucl. Med.* 34, 2216–2221.
- Innis, R.B., Cunningham, V.J., Delforge, J., Fujita, M., Gjedde, A., Gunn, R.N., Holden, J., Houle, S., Huang, S.C., Ichise, M., Iida, H., Ito, H., Kimura, Y., Koeppe, R.A., Knudsen, G.M., Knuuti, J., Lammertsma, A.A., Laruelle, M., Logan, J., Maguire, R.P., Mintun, M.A., Morris, E.D., Parsey, R., Price, J.C., Slifstein, M., Sossi, V., Suhara, T., Votaw, J.R., Wong, D.F., Carson, R.E., 2007. Consensus nomenclature for in vivo imaging of reversibly binding radioligands. *J. Cereb. Blood Flow. Metab.* 27, 1533–1539.
- Jack Jr., C.R., Knopman, D.S., Jagust, W.J., Petersen, R.C., Weiner, M.W., Aisen, P.S., Shaw, L.M., Vemuri, P., Wiste, H.J., Weigand, S.D., Lesnick, T.G., Pankratz, V.S., Donohue, M.C., Trojanowski, J.Q., 2013. Tracking pathophysiological processes in Alzheimer's disease: an updated hypothetical model of dynamic biomarkers. *Lancet Neurol.* 12, 207–216.
- Ji, B., Chen, C.J., Bando, K., Ashino, H., Shiraishi, H., Sano, H., Kasahara, H., Minamizawa, T., Yamada, K., Ono, M., Zhang, M.R., Seki, C., Farde, L., Suhara, T., Higuchi, M., 2015. Distinct binding of amyloid imaging ligands to unique amyloid-beta deposited in the presubiculum of Alzheimer's disease. *J. Neurochem.* 135, 859–866.
- Kadmas, D.J., Rust, T.C., Hoffman, J.M., 2013. Single-scan dual-tracer FLT+FDG PET tumor characterization. *Phys. Med. Biol.* 58, 429–449.
- Kessler, R.M., Ansari, M.S., de Paulis, T., Schmidt, D.E., Clanton, J.A., Smith, H.E., Manning, R.G., Gillespie, D., Ebert, M.H., 1991. High affinity dopamine D2 receptor radioligands. 1. Regional rat brain distribution of iodinated benzamides. *J. Nucl. Med.* 32, 1593–1600.
- Koeppe, R.A., Raffel, D.M., Snyder, S.E., Ficar, E.P., Kilbourn, M.R., Kuhl, D.E., 2001. Dual-[ $^{11}\text{C}$ ]tracer single-acquisition positron emission tomography studies. *J. Cereb. Blood Flow. Metab.* 21, 1480–1492.
- Kung, H.F., Pan, S., Kung, M.P., Billings, J., Kasliwal, R., Reilly, J., Alavi, A., 1989. In vitro and in vivo evaluation of [ $^{123}\text{I}$ ]IBZM: a potential CNS D-2 dopamine receptor imaging agent. *J. Nucl. Med.* 30, 88–92.
- Lammertsma, A.A., Hume, S.P., 1996. Simplified reference tissue model for PET receptor studies. *Neuroimage* 4, 153–158.
- Laruelle, M., 2000. Imaging synaptic neurotransmission with in vivo binding competition techniques: a critical review. *J. Cereb. Blood Flow. Metab.* 20, 423–451.
- Lee, S., Gregor, J., Kennel, S.J., Osborne, D.R., Wall, J., 2015. GATE validation of standard dual energy corrections in small animal SPECT-CT. *PLoS One* 10, e0122780.
- Lee, S., Gregor, J., Osborne, D., Wall, J., 2013. Dual isotope SPECT imaging of I-123 and I-125. In: Nuclear Science Symposium and Medical Imaging Conference (NSS/MIC). IEEE, 2013 IEEE.
- Lukasiewicz, S., Polit, A., Kedracka-Krok, S., Wedzony, K., Mackowiak, M., Dziedzicka-Wasylewska, M., 2010. Hetero-dimerization of serotonin 5-HT(2A) and dopamine D(2) receptors. *Biochim. Biophys. Acta* 1803, 1347–1358.
- Ma, J., Ye, N., Cohen, B.M., 2006. Expression of noradrenergic  $\alpha 1$ , serotonergic 5HT2a and dopaminergic D2 receptors on neurons activated by typical and atypical antipsychotic drugs. *Prog. Neuro-Psychopharmacology Biol. Psychiatry* 30, 647–657.
- Mattner, F., Bandin, D.L., Staykova, M., Berghofer, P., Gregoire, M.C., Ballantyne, P., Quinlivan, M., Fordham, S., Pham, T., Willenborg, D.O., Katsifis, A., 2011. Evaluation of [(1)(2)(3)I]-CLINDE as a potent SPECT radiotracer to assess the degree of astroglia activation in cuprizone-induced neuroinflammation. *Eur. J. Nucl. Med. Mol. Imaging* 38, 1516–1528.
- Mattner, F., Mardon, K., Katsifis, A., 2008. Pharmacological evaluation of [ $^{123}\text{I}$ ]-CLINDE: a radioiodinated imidazopyridine-3-acetamide for the study of peripheral benzodiazepine binding sites (PBBS). *Eur. J. Nucl. Med. Mol. Imaging* 35, 779–789.
- McCormick, P.N., Ginovart, N., Wilson, A.A., 2011. Isoflurane anaesthesia differentially affects the amphetamine sensitivity of agonist and antagonist D2/D3 positron emission tomography radiotracers: implications for in vivo imaging of dopamine release. *Mol. Imaging Biol.* 13, 737–746.
- Meikle, S.R., Kench, P., Kassioti, M., Banati, R.B., 2005. Small animal SPECT and its place in the matrix of molecular imaging technologies. *Phys. Med. Biol.* 50, R45–R61.
- Millet, P., Moulin-Sallanon, M., Tournier, B.B., Dumas, N., Charnay, Y., Ibanez, V., Ginovart, N., 2012. Quantification of dopamine D(2/3) receptors in rat brain using factor analysis corrected [ $^{18}\text{F}$ ]fallypride images. *Neuroimage* 62, 1455–1468.
- Nestler, E.J., Hyman, S.E., 2010. Animal models of neuropsychiatric disorders. *Nat. Neurosci.* 13, 1161–1169.
- Ordóñez, A.A., Pokkali, S., DeMarco, V.P., Klunk, M., Mease, R.C., Foss, C.A., Pomper, M.G., Jain, S.K., 2015. Radioiodinated DPA-713 imaging correlates with bactericidal activity of tuberculosis treatments in mice. *Antimicrob. Agents Chemother.* 59, 642–649.
- Pimlott, S.L., Ebmeier, K.P., 2007. SPECT imaging in dementia. *Br. J. Radiol.* 80 (2), S153–S159.
- Schiffer, W.K., Mirrione, M.M., Biegón, A., Alexoff, D.L., Patel, V., Dewey, S.L., 2006. Serial microPET measures of the metabolic reaction to a microdialysis probe implant. *J. Neurosci. Methods* 155, 272–284.
- Sehlin, D., Fang, X.T., Cato, L., Antoni, G., Lannfelt, L., Syvanen, S., 2016. Antibody-based PET imaging of amyloid beta in mouse models of Alzheimer's disease. *Nat. Commun.* 7, 10759.
- Selvaraj, S., Arnone, D., Cappai, A., Howes, O., 2014. Alterations in the serotonin system in schizophrenia: a systematic review and meta-analysis of postmortem and molecular imaging studies. *Neurosci. Biobehav. Rev.* 45, 233–245.
- Tsartsalis, S., Dumas, N., Tournier, B.B., Pham, T., Moulin-Sallanon, M., Gregoire, M.C., Charnay, Y., Millet, P., 2015. SPECT imaging of glioma with radioiodinated CLINDE: evidence from a mouse GL26 glioma model. *EJNMMI Res.* 5, 9.
- Tsartsalis, S., Moulin-Sallanon, M., Dumas, N., Tournier, B.B., Ghezzi, C., Charnay, Y., Ginovart, N., Millet, P., 2014a. Quantification of GABA<sub>A</sub> receptors in the rat brain with [(123)I]lomazenil SPECT from factor analysis-denoised images. *Nucl. Med. Biol.* 41, 186–195.
- Tsartsalis, S., Moulin-Sallanon, M., Dumas, N., Tournier, B.B., Ginovart, N., Millet, P., 2014b. A modified simplified reference tissue model for the quantification of dopamine D2/3 receptors with [ $^{18}\text{F}$ ]fallypride images. *Mol. Imaging* 13.
- Tsartsalis, S., Tournier, B.B., Huynh-Gatz, T., Dumas, N., Ginovart, N., Moulin-Sallanon, M., Millet, P., 2016a. 5-HT<sub>2A</sub> receptor SPECT imaging with [ $^{123}\text{I}$ ]R91150 under P-gp inhibition with tariquidar: more is better? *Nucl. Med. Biol.* 43, 81–88.
- Tsartsalis, S., Tournier, B.B., Aoun, K., Habiby, S., Pandolfo, D., Dimiziani, A., Ginovart, N., Millet, P., 2017. A single-scan protocol for absolute D2/3 receptor quantification with [ $^{123}\text{I}$ ]IBZM SPECT. *Neuroimage* 147, 461–472.
- Tsartsalis, S., Tournier, B.B., Huynh-Gatz, T., Dumas, N., Ginovart, N., Moulin-Sallanon, M., Millet, P., 2016b. 5-HT<sub>2A</sub> receptor SPECT imaging with [(1)(2)(3)I] R91150 under P-gp inhibition with tariquidar: more is better? *Nucl. Med. Biol.* 43, 81–88.
- Vallez Garcia, D., Casteels, C., Schwarz, A.J., Dierckx, R.A., Koole, M., Doorduyn, J., 2015. A standardized method for the construction of tracer specific PET and SPECT rat brain templates: validation and implementation of a toolbox. *PLoS One* 10, e0122363.
- Varela, M.J., Lage, S., Caruncho, H.J., Cadavid, M.I., Loza, M.I., Brea, J., 2015. Reelin influences the expression and function of dopamine D2 and serotonin 5-HT<sub>2A</sub> receptors: a comparative study. *Neuroscience* 290, 165–174.
- Wu, Y., Carson, R.E., 2002. Noise reduction in the simplified reference tissue model for neuroreceptor functional imaging. *J. Cereb. Blood Flow. Metab.* 22, 1440–1452.
- Xi, W., Tian, M., Zhang, H., 2011. Molecular imaging in neuroscience research with small-animal PET in rodents. *Neurosci. Res.* 70, 133–143.